RHOA Loss of Function Impairs the IFNγ Response and Promotes CD19 Antigen Escape to Drive CAR-T Resistance in Diffuse Large B-cell Lymphoma

Austin D. Newsam[1,2,6,†], Bachisio Ziccheddu[4,6,†], Venu Venkatarame Gowda Saralamma[2,3], Caroline A. Coughlin[1,2,6], Yitzhar E. Goretsky[5], Abdessamad A. Youssfi[2,3], Marco Vincenzo Russo[2], Natalia Campos Gallego[2], Nikolai Fattakhov[2], David G. Coffey[2,4], Daniel E. Tsai[1,2], David Carmona-Berrio[2,6], David M. Suissa[2,6] Paola Manara[2,6], Anya K. Sondhi[2,6], Evan R. Roberts[2,8], Isaiah Sheffield-Veney[9], Jay Y. Spiegel[2,10], Catalina Amador[2,11], Juan Pablo Alderuccio[2,3], Daniel Bilbao[2,7], Michael D. Jain[12], Francesco Maura[2,4,13,†], Frederick L. Locke[12,†], and Jonathan H. Schatz[2,3,†,*]

[1]Medical Scientist Training Program, University of Miami Miller School of Medicine, Miami, FL, USA

[2]Sylvester Comprehensive Cancer Center, University of Miami Miller School of Medicine, Miami, FL, USA

[3]Division of Hematology, Department of Medicine, University of Miami Miller School of Medicine, Miami, FL USA

[4]Myeloma Division, Sylvester Comprehensive Cancer Center, University of Miami, Miami, FL, USA.

[5]MD Program, University of Miami Miller School of Medicine, Miami, FL, USA

[6]Sheila and David Fuente Cancer Biology Graduate Program, University of Miami Miller School of Medicine, Miami, FL, USA

[7]Department of Pathology and Laboratory Medicine, University of Miami Miller School of Medicine, Miami, FL USA

[8]Desai Sethi Urology Institute, Sylvester Comprehensive Cancer Center, University of Miami, Miami, FL USA

[9]University of Miami, Coral Gables, FL USA

[10]Division of Transplant and Cellular Therapy, Department of Medicine, University of Miami Miller School of Medicine, Miami, FL USA

[11]Division of Hematopathology, Department of Pathology, University of Miami Miller School of Medicine, Miami, FL USA

[12]Blood and Marrow Transplant and Cellular Immunotherapy, H. Lee Moffitt Cancer Center and Research Institute, University of South Florida Morsani College of Medicine, Tampa, FL USA

[13]Memorial Sloan Kettering Cancer Center, New York, NY USA

† Authors contributed equally

*Correspondence: jschatz@med.miami.edu

ABSTRACT

CD19-directed chimeric antigen receptor (CAR)-T cells are breakthrough therapies for aggressive B-cell lymphomas, but less than half of patients achieve durable responses. We previously showed through whole-genome sequencing of tumors from CAR-T-treated patients that deletions of *RHOA* (3p21.31) are enriched in cases progressing after treatment. *RHOA*'s roles in resistance and pathogenesis are poorly defined, despite loss-of-function alterations that occur in ~20% of newly diagnosed diffuse large B-cell lymphoma (DLBCL) cases. To evaluate mechanisms of CAR-T resistance, we created RHOA-deficient DLBCL systems and confirmed cell-intrinsic loss of response to CAR-19 in vitro and in vivo. RHOA loss promotes AKT activation that impairs cell-intrinsic responses to interferon gamma (IFNγ). Moreover, expression of the CAR target CD19 is consistently down-regulated accompanied by a drive toward plasmablast differentiation. RHOA deficient tumors demonstrate greatly increased sensitivity to AKT-pathway inhibitors, which reverse impaired IFNγ responses. Lymphoma microenvironments in vivo in immunocompetent mice reveal that RHOA loss promotes decreased infiltration by cytotoxic T cells and enrichment of M2-polarized macrophages, known markers of CAR-T resistance in lymphoma clinical cases. Overall, we characterize RHOA deficiency as an AKT-mediated CAR-T resistance driver and implicate avoidance of T-cell mediated killing as a likely reason for RHOA's frequent loss in DLBCL pathogenesis.

INTRODUCTION

CD19-targeted autologous chimeric antigen receptor T-cell (CAR-19) immunotherapies are potentially curative for patients with aggressive B-cell lymphomas who have not adequately responded to standard chemoimmunotherapy combinations.[1–3] Durable complete response (CR) rates of >30% represent a major breakthrough for these patients, but those with unsatisfactory responses, unfortunately still the majority, have poor prognoses.[4] Detailed comprehension of resistance factors is an urgent priority to inform the design of future therapies able to efficaciously leverage the CAR-T breakthrough to larger numbers of patients. While characteristics of CAR-19 products and lymphoma microenvironments have been well described,[5–8] the functional roles of lymphoma genomes in thwarting CAR-19 responses are minimally explored.

In previous work employing whole-genome sequencing (WGS) on fresh pre-CAR-T tumor samples with matched germline DNA, we showed genomic factors collectively are stronger predictors of outcome than clinical factors like metabolic tumor volume (MTV) or patient age.[9] Additional studies implicate, like ours, that genomic complexity and/or mutation or loss of specific genes can predict CAR-19 outcomes,[10–12] but studies to establish mechanisms of tumor-intrinsic resistance are limited to EZH2 gain-of-function mutations and FAS-mediated extrinsic apoptotic engagement.[13,14]

In addition to markers of genomic complexity, our genomics results implicated a candidate single-gene alteration, del 3p21.31 containing *RHOA*.[9] *RHOA* is frequently altered also in newly diagnosed DLBCL cases, but its roles in pathogenesis remain poorly defined. Predominantly monoallelic 3p21.31 deletions were reported in 118/700 (16.8%) of cases in the recently published multi-institution combined dataset that established the DLBclass molecular disease clusters.[15] These deletions are a defining feature of cluster 2 (C2) cases, while non-synonymous *RHOA* mutations are a defining feature of C1, occurring in 31/700 (4.4%) of cases

overall. These patterns therefore implicate loss of function of the Ras homolog family member A (RHOA) protein since only deletions are found recurrently by genomic copy number analyses, and recurrent mutations are predicted to disrupt RHOA's interactions with activating guanine-exchange factor (GEF) proteins.[16,17]

Specific functional studies on RHOA in DLBCL, however, are lacking, and its potential pathogenic roles are currently defined downstream of other disease-driving alterations. Muppidi and colleagues showed recurrent loss of Gα13 signaling downstream of the S1PR2 and P2RY8 receptors and implicated RHOA as a suppressor of AKT activation as a readout of this tumor-suppressive pathway.[18] Jiang and colleagues revealed RHOA is a key downstream effector of the HGAL tumor suppressor that acts by limiting tumor cell motility.[19] More recently, Sahasrabuddhe and colleagues revealed a novel lymphomagenic pathway that may ironically promote increased RHOA activation.[20] Specifically, loss of the E3 ubiquitin ligase FBXO45 leads to accumulation of the GEF-H1 guanine exchange factor that has RHOA as one of its targets. RHOA activation in this study was used as a readout of GEF-H1 accumulation, however, and was not shown to drive MAPK-dependent lymphomagenesis in the FBXO45-deficient context. Therefore, given the poorly defined roles of a gene selected for deletion or deleterious mutations in ~1 in 5 newly diagnosed DLBCL cases and strong selection for its loss in CAR-T resistant cases, dedicated studies are highly warranted.

In this study, we generated DLBCL RHOA loss-of-function (LoF) systems to elucidate pathways of dependency and mechanisms of immune evasion employed by RHOA-deficient DLBCL. We also used RHOA deficient lymphoma mouse models to study the effects of RHOA loss on the lymphoma microenvironment (LME) and the efficacy of CAR-19 therapy. As in prior studies,[21] complete *RHOA* deletion was not tolerated in DLBCL cells, and our findings therefore characterize it as a DLBCL haploinsufficient tumor suppressor. These studies represent the first direct functional evaluation of a recurrently deleted LBCL gene linked specifically to poor clinical responses to CAR-19.

RESULTS

RHOA deficiency associates with CAR-19 failure and chronically inflamed tumors in LBCL patients

We interrogated whole genome sequencing (WGS) data from 54 patients with relapsed/refractory (r/r) large B-cell lymphoma (LBCL) treated with anti-CD19 CAR T-cell therapy, 49 of whom were included in our previous study.[9] We also analyzed WGS from 96 newly diagnosed B-cell lymphoma patients from the Pan-Cancer Analysis of Whole Genomes (PCAWG) consortium.[22] Of the 150 total cases analyzed, 86 were diffuse large B-cell lymphomas (DLBCL), 45 follicular lymphoma/transformed follicular lymphoma, 3 transformed chronic lymphocytic leukemia, 13 Burkitt lymphoma, 2 marginal zone B-cell lymphoma, and 1 post-transplant lymphoproliferative disorder (Extended Data Table 1). Focusing on the genomic drivers previously associated with clinical outcomes after CART, alterations in *RHOA* (mutations or deletions), APOBEC and SBS18 mutational signatures, and chromothripsis were significantly enriched in r/r LBCL patients treated with CAR-19 ($p < 0.05$; **Fig. 1A**). All these factors retained significance in predicting early relapse after CART (**Extended Data Fig. 1**). Deletion involving 3p21.31 or *RHOA* mutations occurred in 23 patients (22% in CAR-19 [n=12]; 14.7% in PCAWG [n=11], **Fig. 1A**). Among these, monoallelic deletions were present in 78% of cases, monoallelic mutations in 17.4%, and biallelic inactivation in one sample (PCAWG dataset). Although some 3p21.31 deletions also included the *FHIT* tumor suppressor (altered in some digestive-tract tumors[23]), high-resolution analyses revealed that *RHOA* was the minimally deleted region and consistently affected in all cases, with deletions being mainly focal (**Fig. 1B**).

Because RHOA's role in lymphoma pathogenesis has been underexplored, we assessed the consequences of these deletions by analyzing bulk transcriptomic data from 52 CAR-19-treated LBCL samples with paired WGS. As expected, *RHOA* expression was significantly lower in *RHOA*-deleted compared to WT samples (p=0.00017) (**Fig. 1C**).

Additionally, we conducted differential gene expression and gene set enrichment analyses (GSEA) using bulk RNA-seq data from CAR-19-treated LBCL patients. RHOA-deleted cases exhibited enrichment of pathways related to JAK/STAT signaling, MYC targets, PI3K-AKT, and mTORC1 signaling (**Figure 1D**). We examined selected immune-related genes, specifically those associated with MHC Class I *(HLA-A, HLA-B, HLA-C*, and *B2M*). Interestingly, *RHOA* deletions significantly reduced the expression of *HLA-B* ($p = 0.035$; **Figure 1E**), a critical component of the MHC class I complex. In contrast, *FHIT* deletions had no detectable impact on the expression of analyzed genes. Overall, this investigation confirms the role of deletions of 3p21.31 in predicting outcomes in LBCL treated with CART with *RHOA* as the driver gene involved. Interestingly loss of *RHOA* associated with multiple gene signatures in tumors known to play a role in immunotherapy responses.

RHOA LoF drives activation of and reliance on PI3K-AKT-mTOR signaling

We next interrogated the biology of *RHOA* alterations DLBCL by creating murine and human LoF laboratory systems with *RHOA* shRNA knockdown or CRISPR/Cas9 knockout (RHOA LoF hereafter referring to either sg*RHOA* or sh*RHOA*/sh*Rhoa* systems). Loss of function was confirmed via active (GTP-bound) Rho pulldown and recovered upon rescue (**Fig. 2A,** Extended Data Fig. 2). Systems included RIVA, an activated B-cell (ABC) cell of origin (COO) cell line derived from DLBclass C1 (*BCL6* translocation and *NOTCH2* mutation[24]), and SU-DHL-4, a germinal-center B (CGB) COO line derived from C2.[15] Complete loss of *RHOA* never resulted from single-cell selections after sg*RHOA*/Cas9 introduction, consistent with CRISPR screening results reported previously by others,[21] implicating *RHOA* as a haploinsufficient tumor suppressor whose complete absence is not tolerated. These systems therefore recapitulate the near exclusive predominance of monoallelic deletions or LoF mutations in patients' tumors.[22] Only 2/118 (1.7%) of cases with 3p21.31 in the DLBclass combined dataset had biallelic deletions.[15] Previous work showed RHOA gain-of-function recapitulates HGAL-mediated

decreased motility of DLBCL cells in migration assays.[19] We find consistently that RHOA LoF produced opposite effects, increasing cell migration and aggregation in culture (**Fig. 2B, 2C**).

We next assessed the impact of RHOA LoF on tumor cell-intrinsic gene expression. RNA-sequencing comparing RIVA sg*RHOA* to parental RIVA cells revealed upregulation of PI3K/AKT/mTOR pathway-associated gene expression, consistent with prior work implicating RHOA in suppressing AKT downstream of S1PR2/P2RY8 and Gα13 signaling (**Fig. 2D**).[18] Western blotting of RHOA LoF cells confirmed upregulation of pAKT S473 in all engineered systems, suggesting a bona fide role of RHOA as a suppressor of AKT activity in DLBCL (**Fig. 2E**). RHOA LoF promoted increased dependence on PI3K/AKT/mTOR signaling, indicated by significantly greater sensitivity to inhibitors of PI3Kδ (idelalisib), PI3Kδ/γ (duvelisib), AKT (capivasertib), or mTOR (rapamycin) (**Fig. 2F**). *RHOA* re-expression rescued idelalisib sensitivity (**Fig. 2G**). Drug sensitivity and gene expression data[25] from 18 DLBCL cell lines available on the depmap.org portal corroborated the association between decreased *RHOA* expression and increased PI3K (CAL-101), AKT (GSK 690693), and mTOR (A-1065-5) sensitivity (**Fig. 2H**). Mechanistically, wild-type RHOA activates PTEN to suppress PI3K through a ROCK dependent mechanism previously described.[26,27] Our data suggest loss of this activity in clinical DLBCL via *RHOA* monoallelic deletions and LoF mutations promotes a targetable dependence on PI3K activation.

RHOA inactivation impairs the cell-intrinsic interferon gamma response that can be restored with PI3K inhibition

Type I and Type II interferon pathway activation was prominent in bulk RNA-seq of RHOA-deficient tumors (**Fig. 1C**), including the chronic ISG.RS signature associated previously with CAR-19-resistant lymphoma microenvironments.[7] These signatures were notably absent, however, from the up-regulated pathways in RNA-seq comparing RHOA LoF cells to WT (**Fig. 2D**), suggesting impaired responses within tumor cells themselves. Previous work on loss-of-

function Y42C *RHOA* mutations in gastric cancer demonstrated decreased pSTAT1, IRF1, and CXCL10 resulting from upregulated AKT signaling.[28] Interferon regulatory factor 1 (IRF1) is a transcription factor of interferon-stimulated genes (ISGs) including MHC-I antigen presentation genes (*HLA-B,*[29] *TAP2,*[30] *B2M*[31]) and immune effector recruiters (*CXCL9*, *CXCL10*, *CXCL11*[32,33]) and is activated via JAK2-STAT1 signaling in response to IFNγ.[34] In the noncanonical pathway of JAK-STAT signaling from IFNγ, JAK2 signals through proline-rich tyrosine kinase 2 (PYK2) to activate glycogen synthase kinase 3 beta (GSK3β), a regulator of STAT1 activation,[34] and AKT as a direct inhibitor of GSK3β via S9 phosphorylation.[34,35] Thus, we hypothesized that increased AKT activity in tumor cells driven by RHOA LoF in DLBCL decreases transcription of STAT1 induced gamma-activated sequences (GAS), such as *IRF1*, circumventing IFNγ mediated immunorecognition (Extended Data Fig. 3). Strikingly, GSEA analysis of down-regulated genes comparing RIVA sg*RHOA* to WT revealed pronounced depletion of interferon gamma and alpha responses (**Fig. 3A)**, in marked contrast to bulk assessment of overall clinical tumors (**Fig. 2D**). We confirmed specific loss of *IRF1*, *STAT1*, and *CXCL10* (**Fig. 3B**), including significant reduction in CXCL10 secretion (**Fig. 3C**).

To functionally validate impaired IFNγ responses, we treated WT and RHOA LoF systems with IFNγ (30 ng/mL) and assessed transcription and translation of key type 2 interferon regulatory factors. RHOA LoF cells showed significantly impaired up-regulation of *STAT1* and *IRF1* transcripts 2 hours after IFNγ stimulation (**Fig. 3D**). MHC-I/B2M induction to increase immune visibility is a crucial response of IFNγ mediated antitumor immunity[30] and under basal conditions, RHOA LoF cell lines expressed similar levels of MHC-I as their parental counterparts (Extended Data Fig. 4A, Note: OCI-Ly1 lacks expression of MHC-I and is considered among the nearly 50% of MHC-I deficient DLBCLs.)[36] However, when treated for 48 hours with IFNγ we found significantly reduced upregulation of MHC-I based on detection of the obligate light chain B2M on the cell surface in response to IFNγ exposure (**Fig. 3E**). To interrogate relevance of these findings during immune-mediated cytotoxicity, we assessed cell

surface MHC-I induction during coculture with activated PBMCs. RHOA-deficient cells showed reduced MHC-I induction during co-culture compared to WT cells, and this was due to IFNγ as a blocking antibody abrogated response (**Fig. 3F**). This associated specifically with aberrant IFNγ responses, as interferon-gamma receptor (IFNGR) levels were the same in parental and RHOA LoF cells (Extended Data Fig. 4B).

To assess mechanistically if AKT activation in RHOA LoF lymphoma cells was responsible for faulty IFNγ responses, we pretreated cells with idelalisib (1μM) or DMSO for 24 h and then stimulated with IFNγ (30 ng/mL) for 2 h. Pretreating with idelalisib enhanced IFNγ-stimulated IRF1 expression across systems, specifically in RHOA LoF (**Fig. 3G**). Together, these data suggest RHOA inactivation plays a causal role in blocking IFNγ signaling leading to diminished MHC-I antigen display, and that inhibiting AKT with PI3K inhibitors can restore IRF1 expression leading to IFNγ mediated immunorecognition.

RHOA loss fosters immunosuppressive lymphoma microenvironments

We then explored how impaired IFNγ responses downstream of RHOA deficiency impact the lymphoma microenvironment (LME). We created syngeneic RHOA-deficient lymphoma murine models by engrafting A20 sh*Rhoa* and A20 sh*Renilla* cells into strain-matched recipients and harvested engrafted tumors for single-cell RNA sequencing. We observed a stark difference in transcriptional profiles between A20 sh*Rhoa* and A20 parental lymphoma B cells (**Fig. 4A**), with GSEA analysis revealing upregulated mTOR signaling and downregulated interferon gamma responses similar to the RNA-seq analyses on cultured RIVA sg*RHOA* cells (**Fig. 4C**). Loss of IFNγ response was therefore a consistent finding in lymphomas present in immunocompetent microenvironments, a known driver of CAR-T resistance.[37] Analyses confirmed persistent knockdown of *Rhoa* expression in these tumors as well as deficient expression of *B2m* and class I MHC HLA-A ortholog *H2-K1* (**Fig. 4D**). We also investigated expression of the CD19 CAR target and found strikingly decreased *Cd19*

expression in the sh*Rhoa* tumor cells (**Fig. 4D,** further characterized below). While the LME was relatively immune depleted in both genotypes (**Fig. 4B**), the most abundant non-B cell in the LME was T-cells, comprising 6.5% and 4.7% of total annotated cells in A20 parental and A20 sh*Rhoa* tumors, respectively (Extended Data Fig. 5A). This statistically insignificant difference in T cell abundance was supported ex vivo by analyzing CD3+ composition of viably frozen tumors (Extended Data Fig. 5B) and supports current thinking that the ratio and proportion of activated CD8+ T cells predicts immune deregulated LMEs more than global T cell infiltration.[6,8] Differential expression of transcripts in T cells revealed downregulation of *Cxcl10* giving way also to downregulated *Cd8a* and *Prf1* expression. Upregulated genes alternatively revealed enriched *Foxp3* and *Cd4* (**Fig. 4E**). GSEA of bulk annotated T-cells also revealed forkhead box transcription factor (*FOXP3*) targets highly enriched in RHOA deficient tumors (**Fig. 4F**), a marker of CD4+ CD25+ regulator T cells (Tregs).[38] While differential abundance analysis of CD4+ FoxP3+ Tregs did not reach significance in A20 sh*Rhoa* LMEs, there was a noticeable trend for enrichment (Extended Data Fig. 5C). When measuring the abundance of T-cell subsets, we found a significant increase in the CD4:CD8 T-cell ratio in sh*Rhoa* tumors compared to controls (**Fig. 4G**). This is consistent with the T cell expression data and our *in vitro* findings of significantly decreased CXCL10 (IP-10) secretion from RHOA LoF cells (**Fig. 3C**), as CXCL10 has been documented as a key chemoattractant for CD8 T-cells and is linked to immune-permissive tumor microenvironments.[39,40] Finally, when examining macrophages we found upregulated IL-1ß signaling and de-enriched M1 polarization gene sets (**Fig. 4H**). The IFN-activated macrophage gene *Siglec1,* known to be enriched in LBCL microenvironments with poor CAR-19 responses,[7] was significantly upregulated in sh*Rhoa* tumors (**Fig. 4I**). Together, these findings support the notion that RHOA deficient lymphoma establishes chronically inflamed exhausted LMEs, limiting recruitment of endogenous effector cells, along with tumor cells displaying significantly impaired IFNγ responses.

CD19 surface density is diminished in RHOA-deficient DLBCL

Complete loss of CD19 is uncommon in CAR-19 resistant LBCL, but reduced cell-surface density may correlate with impaired responses.[41] A recent study showed overexpression of the YTHDF2 epitranscriptomic reader can reduce CD19 expression, though alterations to its encoding gene have not been detected in genomics studies of CAR-19 resistance.[42] Additional genomic drivers of this phenomenon are unknown since *CD19* alterations are rarely detected. We therefore further pursued the finding of decreased *Cd19* expression in vivo in sh*Rhoa* A20 cells by assessing CD19 across our human and mouse RHOA LoF systems. Using phycoerythrin quantitative flow cytometry, we determined the number of CD19 molecules per cell to be significantly less in all RHOA LoF cell lines compared to corresponding parental cells (**Fig. 5A**). Western blotting and qPCR suggested these effects occur at a gene-expression level rather than impaired translation or membrane trafficking (**Fig. 5B-C**). Inducible sh*RHOA* cells also demonstrated decreased CD19 bulk protein and membrane levels after doxycycline induction while RHOA rescue partially restored CD19 (**Fig. 5D,** Extended Data Fig. 6A). Likewise, a RHOA-specific inhibitor caused dose-dependent CD19 loss in parental DLBCL cells (Extended Data Fig. 6B). Further, we found strong correlations between *RHOA* and *CD19* transcripts in newly diagnosed DLBCL clinical samples (PCAWG) (**Fig. 5E**).

Previous reports showed loss of Gα13 (*GNA13*) leads to proliferation and loss of confinement of germinal center B-cells in lymphoid organs.[18,43] P2RY8 is a Gα13 protein-coupled receptor upstream that signals through Gα13 and ARHGEF1 to activate RHOA.[18] *P2RY8* mutations detected in circulating tumor DNA associate with impaired event-free survival after CAR-19 in LBCL, with a significant trend also for *GNA13* that encodes Gα13.[12] Recent work investigating P2RY8 variants in lupus uncovered critical roles in restraining plasma cell formation due to suppressed AKT activity.[44] Thus, we hypothesized that RHOA loss may lead to decreased CD19 levels by signaling for a plasmablast phenotype due to significantly upregulated pAKT levels. To test this, we isolated naïve B cells from WT C57BL/6J mice and

transduced with sh*Rhoa*-GFP or sh*Renilla*-GFP retroviral constructs after lipopolysaccharide stimulation and assessed CD138 (syndecin-1) expression 72 h later, as described previously.[44] Viable GFP+ sh*Rhoa* B-cells expressed significantly more CD138 than GFP+ sh*Renilla* B-cells (**Fig. 5F,** Extended Data Fig. 6C gating strategy). Our RIVA bulk RNA-seq data also reported decreased CD138 (*SDC1*) in RHOA LoF (**Fig. 5G**). Strong correlations were also found in the PCAWG data set between *RHOA* and *PRDM1* and *IRF4*, master transcriptional regulators of differentiation along the plasma cell lineage (**Fig. 5H**).[45] Neither PI3K, AKT, or mTOR pathway inhibitors restored CD19 expression in our RHOA LoF systems, suggesting irreversibility of plasmablast differentiation as a driver of reduced CD19 (Extended Data Fig. 6D).

Together, these findings suggest RHOA deficiency promotes CD19 downregulation at the level of transcription associated with induction of plasmablast differentiation, resulting in decreased membrane density of CD19, a known marker of resistance to CAR-19 therapy.

CAR-19 cytotoxicity is impaired against RHOA-deficient lymphomas

To test if RHOA loss provides intrinsic resistance to CAR-19, we performed coculture cytotoxicity assays with human and mouse RHOA LoF lymphoma cells. CAR-19 killing was significantly reduced in all RHOA LoF systems. Using flow cytometry, impedance, and luminescence-based cytotoxicity assays, we observed decreased lysis of human and murine RHOA LoF lymphoma cells across a range effector to target ratios (E:T) (**Fig. 6A**). Interestingly, differential killing was much greater when purified (GFP+) CAR-19 cells were used as opposed to bulk transduced cells (40-50% GFP+) (Extended Data Fig. 7A). While WT cells showed increased sensitivity to the purified product, sg*RHOA* cells experienced no significant increase in cell lysis (**Fig. 6B**). This suggests CD19 downregulation is a key mechanism by which RHOA LoF cells resist engagement by CAR-expressing cells specifically. Indeed, an ELISA for IFNγ revealed significantly decreased levels of IFNγ in supernatants of CAR-19 and RHOA LoF

cocultured cells compared to parental cells (**Fig. 6C**), suggesting less CAR engagement and activation. Target cells themselves did not secrete IFNγ (Extended Data Fig. 7B).

We next assessed if there was differential efficacy of CAR-19 cells against RHOA LoF tumors in vivo (**Fig. 6D**). Parental OCI-Ly1 cells engrafted by tail vein injection to NSG mice showed significant response to treatment with 10^6 purified CD28-costimulated CAR-19 cells, including tumor volume reduction and significantly improved survival compared to untreated tumors (median OS 61 days vs. 34 days for untreated, p=0.0053, **Fig. 6E)**. Animals engrafted with Ly1 sg*RHOA* by contrast experienced no significant benefit from treatment under the same conditions (median 58.5 days vs. 75 for untreated, ns p=0.208, **Fig. 6F**). Indeed, the CAR-T-treated animals if anything died sooner at similar tumor volumes compared to untreated, suggesting CAR-T toxicity is more prominent than efficacy when deployed against RHOA-deficient tumors, though the trend in OS difference did not reach statistical significance. Collectively, these data demonstrate that RHOA loss in LBCL cells promotes inherent resistance to killing by CAR-19 cells in vitro and in vivo.

DISCUSSION

Strategies to improve efficacy of CAR-19 for LBCL include the addition of dual-targeting or novel CARs,[46,47] improving CAR-19 infusion product fitness and production times,[48,49] and implementing neo-adjuvant or combination therapies.[46,50,51] These approaches rooted primarily in CAR-product improvements are largely uninformed by functional studies assessing mediators of CAR-19 resistance encoded by lymphoma genomes. Herein, we describe for the first time, to our knowledge, a single-gene deletion in lymphoma genomes provides tumor-intrinsic resistance mechanisms to evade CAR-19 cells. Specifically, we demonstrate how inactivation of the small GTPase, RHOA, can 1) diminish IFNγ responses in lymphoma target cells 2) promote CD19 antigen escape and 3) foster immunosuppressive lymphoma microenvironments. Elegant

studies of EZH2 inhibitors demonstrated recently that these compounds counteract repression of pro-immune response factors in lymphoma cells with gain-of-function EZH2 mutations and simultaneously directly improve characteristics and function of cytotoxic T-cell effectors.[13] *EZH2* mutations to date, however, have not emerged as resistance markers in CAR-19 genomics studies. In addition, we note that RHOA loss-of-function is largely non-overlapping, with only 1/23 *RHOA* mutant cases in our data derived from the EZB LymphGen group in which *EZH2* mutations are found (**Fig. 1A**). In DLBclass, *EZH2* mutations occur in C3 cases while, as noted above, *RHOA* alterations are in C1 (mutations) and C2 (deletions).[15]

RHOA has been minimally explored in DLBCL despite alterations (monoallelic deletions or LoF mutations) occurring in about 20% of patients.[16] Interestingly, previous CRISPR screening implicated *RHOA* as a candidate DLBCL oncogene as its complete deletion was not tolerated.[21] Our data confirm that complete loss is not tolerated in DLBCL cell lines – countless single-cell selections after sg*RHOA*/Cas9 introduction to bulk cultures never resulted in viable cells with biallelic deletion (**Fig. 2A** and data not shown). Instead, we define *RHOA* as a haploinsufficient tumor suppressor recurrently selected for a reduction in gene dose, recapitulating the near-exclusive predominance of mono-allelic alterations in clinical samples. The separation of function between DLBCL tumor suppression and required minimal functions of RHOA is outside our current scope, representing a fascinating future direction for further research. The only available literature describing the role of RHOA LoF in DLBCL comes from effects downstream of Gα13 or HGAL activation. *GNA13* is a hallmark tumor suppressor in DLBCL that encodes the Gα13 protein and signals through ARGEF1 to activate RHOA.[18] *GNA13* deficient mice develop distinct germinal center B cell dissemination into the blood and it was found that RHOA inactivation downstream of aberrant Gα13 signaling suppressed AKT function.[18] *HGAL* is also a well-known tumor suppressor in DLBCL, and Jiang et al. discovered a role for RHOA in limiting cell motility downstream of HGAL-induced activation of RhoGEFs, increasing GDP-GTP exchange and activating RHOA.[19] We modeled increased AKT activation

and cell motility in multiple systems in which this was a consistent finding due to RHOA LoF. This also resulted, however, in a profound sensitivity to PI3K, AKT, and mTOR inhibitors, suggesting an induced dependence of RHOA deficient lymphomas on this pathway.

We also found AKT activation by RHOA LoF drives dampened IFNγ signaling response in DLBCL cells. Previous work studying RHOA LoF mutations in gastric cancer suggested that increased PI3K-AKT-mTOR signaling suppressed JAK2-GSK3β -STAT1 activation of IRF1, resulting in reduced CXCL10 and effector T cell recruitment.[28] Likewise, we found that loss of RHOA leads to decreased *IRF1* and ISG s involved in antigen presentation such as *HLA-B* and *B2M*. Interestingly, when pretreating RHOA LoF cells with a PI3K inhibitor before stimulating with exogenous IFNγ, we overserved an enhanced restoration of IRF1, supporting the notion that PI3K inhibition can restore sensitivity to IFNγ responses. Interestingly, tumors with *RHOA* deletion or mutation demonstrate increased inflammatory gene-expression patterns including Type I and II interferon pathway activation at the level of bulk-tumor RNA sequencing (**Fig. 1C**). Chronic activation of these pathways in LBCL tumor microenvironments is well-established as a marker of CAR-19 resistance. Tumor cell-intrinsic impairment of IFNγ responses therefore facilitate their survival in this milieu.

Despite a predominance of literature supporting the essential function of IFNγ in controlling tumor growth,[52,53,54] recent work suggests that IFNγ may be dispensable for CAR-19 efficacy in hematologic malignancies.[55,56] By creating IFNγKO CAR-19 cells, Bailey et al. show that CAR-19 killing is unaffected by diminished IFNγ in xenograft models of lymphoma. While CD19 engagement resulting in granzyme and perforin secretion is certainly a major mechanism of contact-dependent target cell death, IFNγ secreted from CAR-19 cells has been documented to play important roles in 1) upregulating the Fas cell surface death receptor (FAS),[14] 2) priming target cells for cytotoxic T cell killing via upregulated MHC-I and 3) enhancing endogenous T and NK cell killing within the LME.[37,52,57] Lack of immunocompetent microenvironments in these studies excluded the well-documented IFNγ-mediated roles of endogenous non-CAR T-cell

activation in lymphoma TMEs during successful CAR-19 responses.[6,8] Therefore, given that most CAR-19 products manufactured for clinical use are heterogenous products consisting of CD4+ and CD8+ CAR-19+ and CAR-19- T cells, and that the authors used purified IFNγKO CAR-19 cells in NSG mice, the importance of IFNγ secreted from both CAR-19 and secondarily activated non-CAR T cells cannot be discounted. Additionally, the authors used Raji (Burkitt lymphoma) and JeKo-1 (mantel cell lymphoma) cell lines for their xenograft studies, which do not fully represent the biology of diffuse large B cell lymphomas. Based on these findings together with our data here presented, we believe impaired IFNγ response downstream of RHOA LoF likely plays key roles both in CAR-19 resistance and in avoidance of immune surveillance in DLBCL pathogenesis.

Less controversial in CAR-19 resistance is CD19 antigen loss, which we show for the first time is a consistent finding downstream of RHOA LoF. CD19 antigen escape is well documented in B-cell acute lymphoblastic leukemia (B-ALL) treated with CD19-directed immunotherapies, where defects in alternative splicing and transcriptional activators may occur.[58,59,60]. However, in DLBCL the incidence and implications of CD19 antigen loss are less clear. The largest case series to document CD19 alterations in CAR-19 treated DLBCL found pretreatment CD19 immunohistochemistry (IHC) H-scores unpredictive of disease progression[41]. However, when looking at CD19 site density by quantitative flow cytometry, nearly half of patients with lymphomas that relapsed displayed significantly less CD19 molecules. This concept of emerging CD19 loss, termed $CD19^{low}$, in the CAR-19 relapsed setting has been corroborated in other studies and highlights the selective pressure of CAR-19 on $CD19^{low}$ tumors[61,12]. We found significantly downregulated CD19 on all RHOA LoF systems generated, one of which had as little as 2000 molecules per cell (Ly1 RHOA LoF, **Fig. 3D**). Unsurprisingly, this was also the most resistant RHOA LoF lymphoma cell line to CAR-19 cells in co-culture studies (**Fig. 4A**). We found CD19 downregulation to be regulated at the level of transcription in RHOA LoF cells and observed a strong correlation between *RHOA* and *CD19*

transcripts in clinical DLBCL samples. The mechanism of CD19 loss in RHOA deficient lymphoma remains incompletely understood, but may be due to AKT activation promoting plasmablast differentiation.

RHOA deficiency blunted CAR-19 killing of DLBCL cells in vitro and in vivo. Using single-cell transcriptomics, we observed that RHOA deficient lymphoma tumors in immunocompetent mice form immunosuppressive LMEs significantly enriched CD4+ T cells. GSEA of annotated T cells also reported highly upregulated gene sets of FoxP3 targets. Together, these data suggest that RHOA deficient lymphoma promotes exhausted LMEs favoring Treg infiltration, likely due to an aberrant inflammatory response in tumor cells driven by unrestrained pAKT activity.

In summary, this work provides evidence that RHOA inactivation is a critical driver of poor CAR-19 efficacy in DLBCL by suppressing IFNγ responses and downregulating CD19. The former provides shelter from surveilling endogenous CD8+ T cells while the latter prevents CAR-19 engagement. Our work supports a growing body of literature suggesting that CAR-19 success is driven as much by an invigoration of endogenous immunity and innate cytotoxic mechanisms as is by CAR-19 cells themselves[14,52,8]. Future studies should examine the mechanism of how MHC-I loss in DLBCL is permitted in situ, as this is a critical mechanism of resistance of endogenous and T-cell directed immunotherapies.

DATA AVAILABILITY

Lead contact – requests for further information and resources should be directed to Dr. Jonathan Schatz (jschatz@miami.edu)

Materials availability – The cell lines, plasmids, and other reagents are available from the lead contact with completed materials transfer agreement

Data and code availability – the WGS, RNA, and scRNA-sequencing data are in process to be submitted to FigShare.

ACKNOWLEDGEMENTS

We wish to thank Dr. Marco Davila for graciously providing the m1928z vector and Mr. Adnan Mookhtiar for sharing expertise of murine HSC culturing and lentiviral preparation. This work was supported by the US Department of Defense Congressionally Directed Medical Research Program (CDMRP) under award GR023242 to J.H.S. Research in this publication was performed in part at the Cancer Modeling, Flow Cytometry, and Onco-Genomic Shared Resources (CMSR RRID: SCR022891, FCSR RRID: SCR022501, OGSR RRID: SCR022502) of the Sylvester Comprehensive Cancer Center at the University of Miami, which is supported by the US NIH National Cancer Institute under award P30CA240139. F.L.L. is a Leukemia and Lymphoma Society Scholar in Clinical Research. F.M. is supported by NIH-NCI, LLS and Department of Defense. Sample collection at Moffitt Cancer Center was supported in part by the US NIH National Cancer Institute (P30CA076292). It is also supported by the Mark Foundation, Bankhead-Coley Cancer Research Program. The content is solely the responsibility of the authors and does not necessarily represent official views of the NIH.

AUTHOR CONTRIBUTIONS

A.D.N., B.Z., J.Y.S., C.A., J.P.A., M.D.J., F.M., and J.H.S. conceived and designed the project. A.D.N., B.Z., V.V.G.W., C.A.C., Y.E.G., I.S., D.E.T., and P.M. designed or conceptualized experiments. M.V.R., D.G.C., D.B., F.M., and J.H.S. supervised experiments. B.Z. and A.A.Y conducted WGS, RNA-seq, and bioinformatic analysis of patient data. A.D.N. performed most of the wet lab experiments, as well as the bulk RNA-seq and scRNA-seq analysis. V.V.G.S., C.A.C., Y.E.G., D.B.C., D.M.S., and A.K.S. performed partial experiments and/or data analysis. N.C.G., N.K., E.R.R., and D.B. performed the mouse experiments. M.D.J., C.A., and F.L.L collected and provided patient data. A.D.N. drafted the manuscript and J.H.S. edited the

manuscript with input from all authors, and all authors have approved the final version of the manuscript.

DECLARATION OF INTERESTS

M.D.J. declares consultancy/advisory for Kite/Gilead and Novartis and research funding (Inst) from Kite/Gilead, Incyte, and Lilly. F.L.L reports a consulting or advisory role for A2, Adaptive, Adaptimmune, Allogene, Amgen, Bluebird Bio, Bristol Myers Squibb/Celgene, Caribou, ecoR1, Gerson Lehman Group, Iovance, Janssen, Kite a Gilead Company, Legend Biotech, Novartis; research funding from the US NIH National Cancer Institute (grants RO1CA276040, RO1CA244328, and P30CA076292), Leukemia and Lymphoma Society, Allogene, BMS, Novartis, 2Sevnty Bio, Kite, and Novartis; and patents, royalties, other intellectual property in the field of cellular immunotherapy. J.P.A. declares research funding from ADC Therapeutics, Genmab, AbbVie, and BeiGene and consultancy or advisory from ADC Therapeutics, Genentech, Genmab, AbbVie, Novartis, Lilly, and Regeneron. F.M. received honoraria from Medidata and Sanofi. J.Y.S. served on an advisory board for Kite. All other authors declare no competing interests.

FIGURES

FIGURE 1

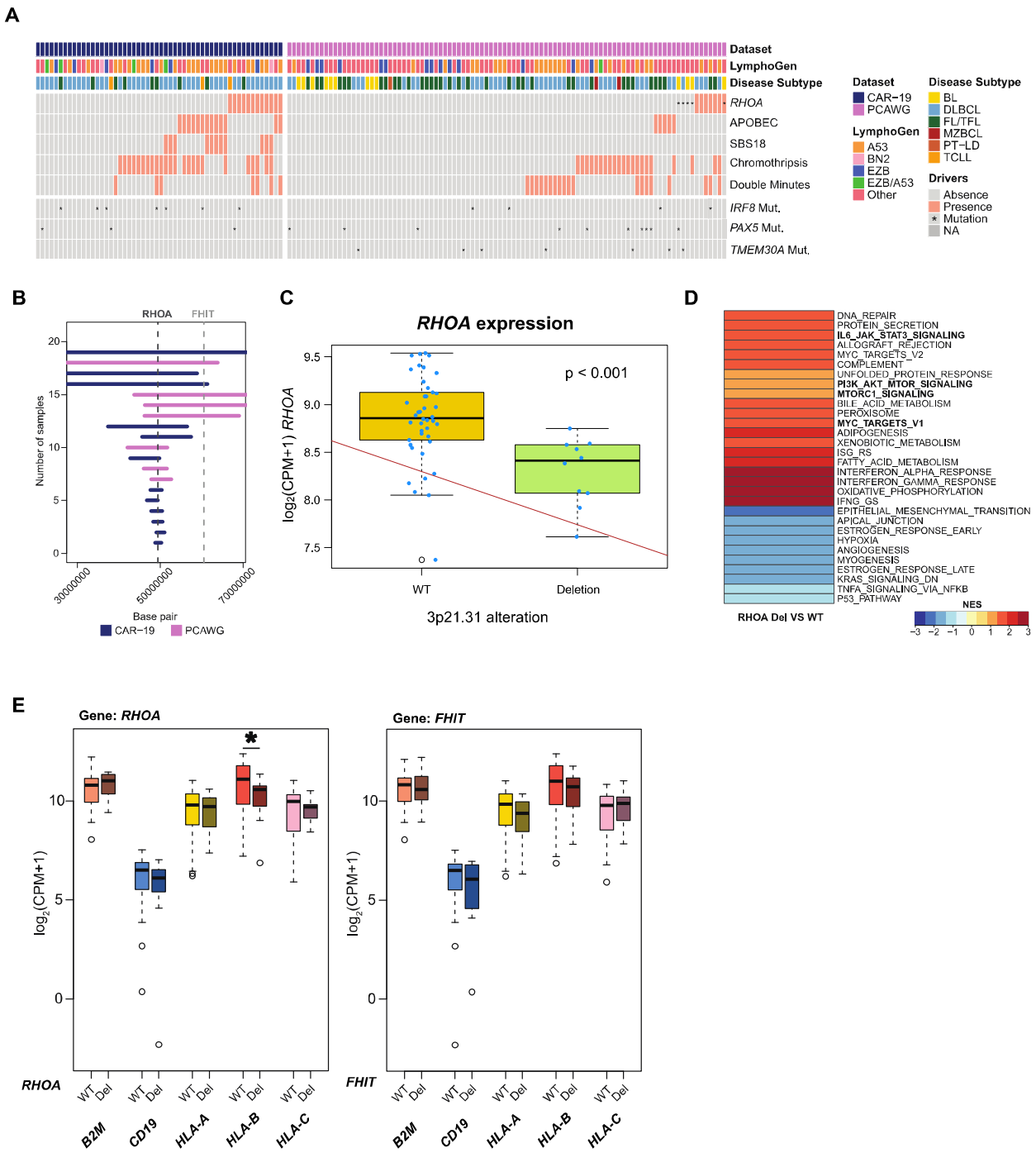

Figure 1: Genomic and transcriptomic analysis in CAR-19 and PCAWG LBCL datasets. A) Heatmap displaying genomic drivers associated with poor outcome to anti-CD19 CART cell therapy. Each column represents a patient (CAR-19 and PCAWG datasets), and each row correspond to a genomic driver or annotation. 'Presence' and 'Absence' are used to identify copy-number variations, mutational signatures, structural variants, and complex events. 'Mutation' specifically indicates non-synonymous mutations. The list of driver genes was generated by combining Jain et al. *Blood* 2020 and Sworder et al. *Cancer Cell* 2023. **B)** Segmentation plot highlighting genomic regions involving *RHOA* and *FHIT* deletions across samples from CAR-19 and PCAWG datasets. The y-axis represents the samples, and the x-axis shows the genomic region coordinates. **C)** Boxplot showing the *RHOA* expression levels based on the 3p21.31 deletion status. Each dot represents an individual patient. The red line indicates the regression trend ($p<0.05$). P-value computed using Wilcoxon test. **D)** Heatmap illustrating significant pathways (FDR<0.05) identified through Gene Set Enrichment Analysis. Pathways of particular interest are shown in bold. **E)** Boxplots comparing expression levels of MHC Class I genes (*HLA-A*, *HLA-B*, *HLA-C*, and *B2M*) and *CD19* in CAR-19 samples with *RHOA* deletions versus WT and *FHIT* deletions versus WT. Significant difference (Wilcoxon test; $p=0.035$) is marked with an asterisk (*).

509 **FIGURE 2**

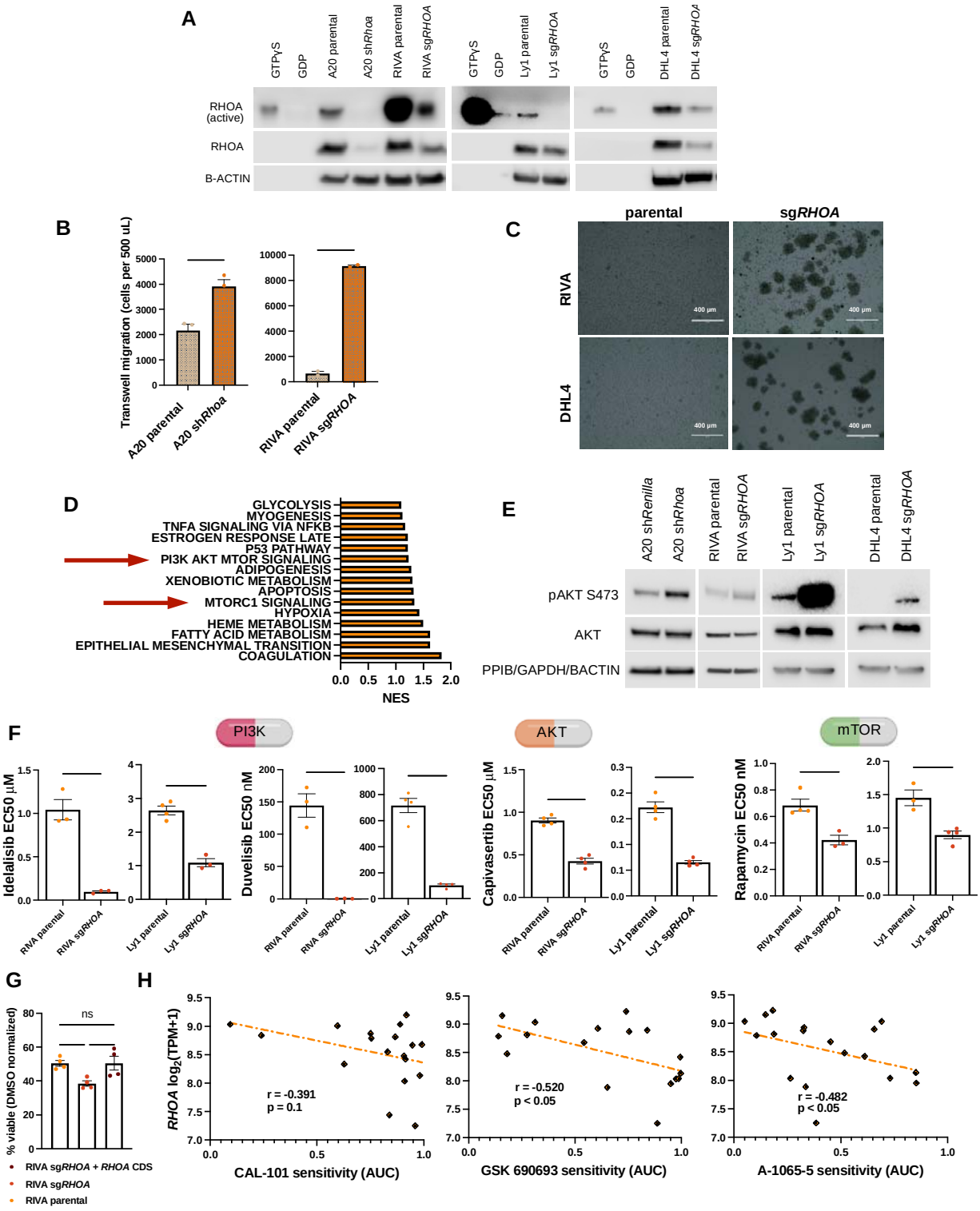

510

Figure 2: RHOA LoF promotes reliance on PI3K/AKT/mTOR signaling. A) Western blot of human and murine engineered RHOA LoF systems (n=4) revealing decreased active RHOA. GTPγS and GDP serve as positive and negative controls for the pulldown, respectively. **B)** Cell migration assay with RHOA LoF cells after 4 h. Number of cells migrated calculated as total events recorded in 500 uL of sample from bottom chamber via flow cytometry. **C)** Light microscopy (10x) images of WT and RHOA LoF cells. **D.** GSEA of RIVA RHOA LoF cells compared to RIVA parental cells using the Hallmark gene set (NES > 1.0). **E)** Western blot of AKT and pAKT levels in LoF cells. **F)** EC50 of RHOA LoF cells after treatment with PI3K, AKT, or mTOR inhibitors for 72 hours. **G)** Cell viability (idelalisib 0.315 μM) of RIVA RHOA rescue cells compared to WT and sg*RHOA* cells. B,F, and G data representative of mean ± SEM of 2-4 independent experiments and analyzed with Student's t-test and one-way ANOVA, respectively. **H)** Drug sensitivity correlations with *RHOA* expression in 18 DLBCL cell lines. r = Spearman's correlational coefficient. NES - normalized enrichment score. (* $p<0.05$ ** $p<0.01$ *** $p<0.001$ **** $p<0.0001$)

FIGURE 3

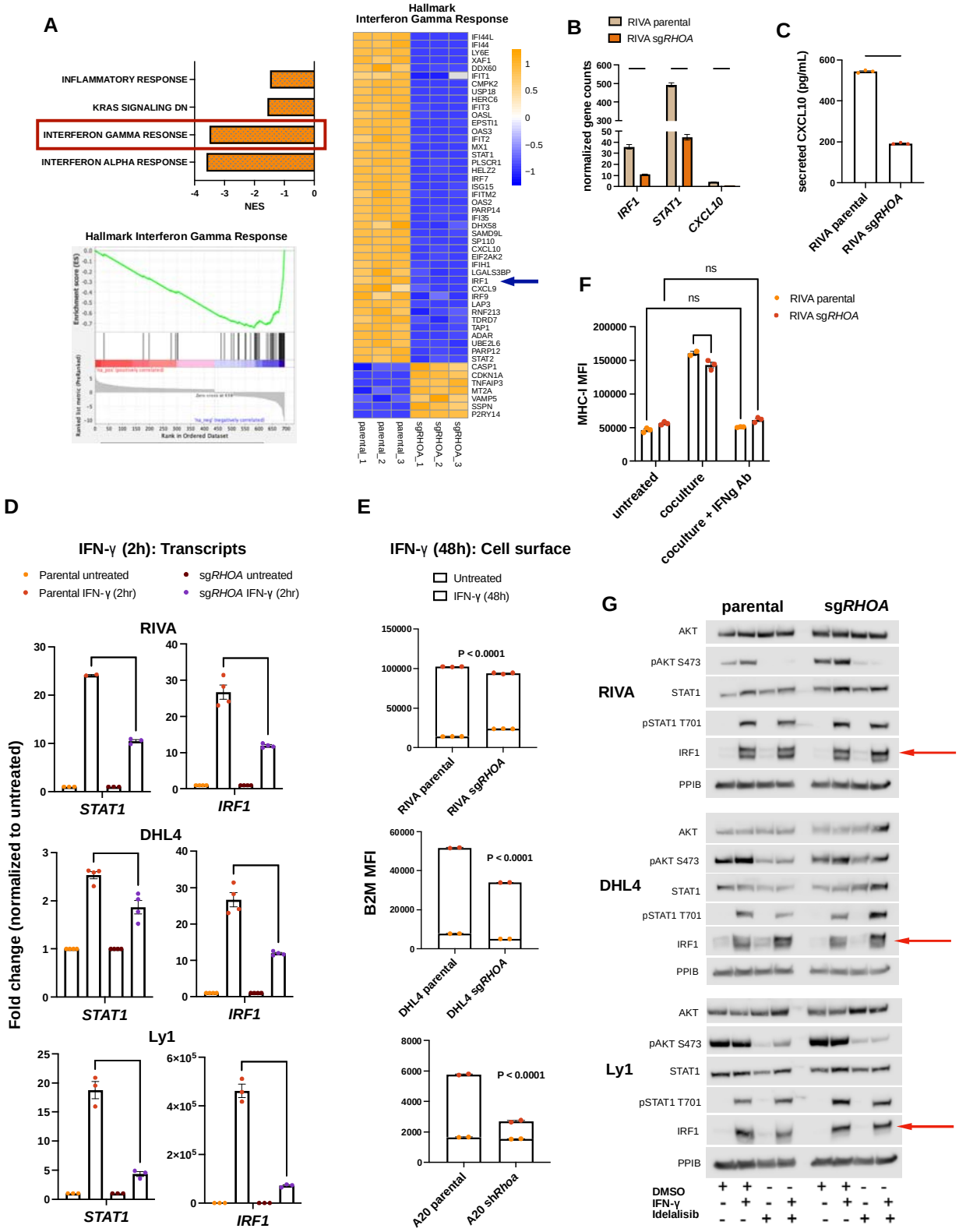
A
INFLAMMATORY RESPONSE
KRAS SIGNALING DN
INTERFERON GAMMA RESONSE
INTERFERON ALPHA RESPONSE
NES
Hallmark Interferon Gamma Response
Hallmark
Interferon Gamma Response
B
RIVA parental
RIVA sgRHOA
normalized gene counts
IRF1
STAT1
CXCL10
C
secreted CXCL10 (pg/mL)
RIVA parental
RIVA sgRHOA
F
ns
ns
RIVA parental
RIVA sgRHOA
MHC-I MFI
untreated
coculture
coculture + IFNg Ab
D
IFN-γ (2h): Transcripts
Parental untreated
Parental IFN-γ (2hr)
sgRHOA untreated
sgRHOA IFN-γ (2hr)
RIVA
DHL4
Ly1
STAT1
IRF1
Fold change (normalized to untreated)
E
IFN-γ (48h): Cell surface
Untreated
IFN-γ (48h)
P < 0.0001
B2M MFI
RIVA parental
RIVA sgRHOA
DHL4 parental
DHL4 sgRHOA
A20 parental
A20 shRhoa
G
parental
sgRHOA
RIVA
DHL4
Ly1
AKT
pAKT S473
STAT1
pSTAT1 T701
IRF1
PPIB
DMSO
IFN-γ
Idelalisib

Figure 3: RHOA inactivation diminishes IFNγ responses that are restored with PI3K inhibition. A) GSEA of RIVA RHOA LoF cells compared to RIVA parental cells using the Hallmark gene set (NES < -1.0) and corresponding heatmap of genes in Interferon Gamma Response gene set (scale = $\log_2$FC). **B)** Normalized gene counts (CPM) of selected genes from RIVA RNAseq analysis. **C)** ELISA of CXCL10 in supernatants from cultures of unstimulated parental and sg*RHOA* RIVA cells. **D)** Transcript levels of ISGs in RHOA LoF cells after treated with 30 ng/mL IFNγ for 2 h. **E)** B2M membrane levels at baseline (untreated) and after incubation with IFNγ (30 ng/mL) for 48 h. Statistical analysis reflects comparison of % change in B2M from baseline between WT and RHOA LoF cells. **F)** Flow cytometry analysis of MHC-I induction after PBMC couture for 40 h. C-H data representative of mean ± SEM of 2-4 independent experiments and analyzed with Student's t-test. **G)** Western blot of RHOA LoF cells pretreated with either DMSO or 1 µM idelalisib (24 h) and then stimulated with IFNγ (30 ng/mL) for 2 h. NES - normalized enrichment score (**p<0.01 ***p<0.001 ****p<0.0001)

FIGURE 4

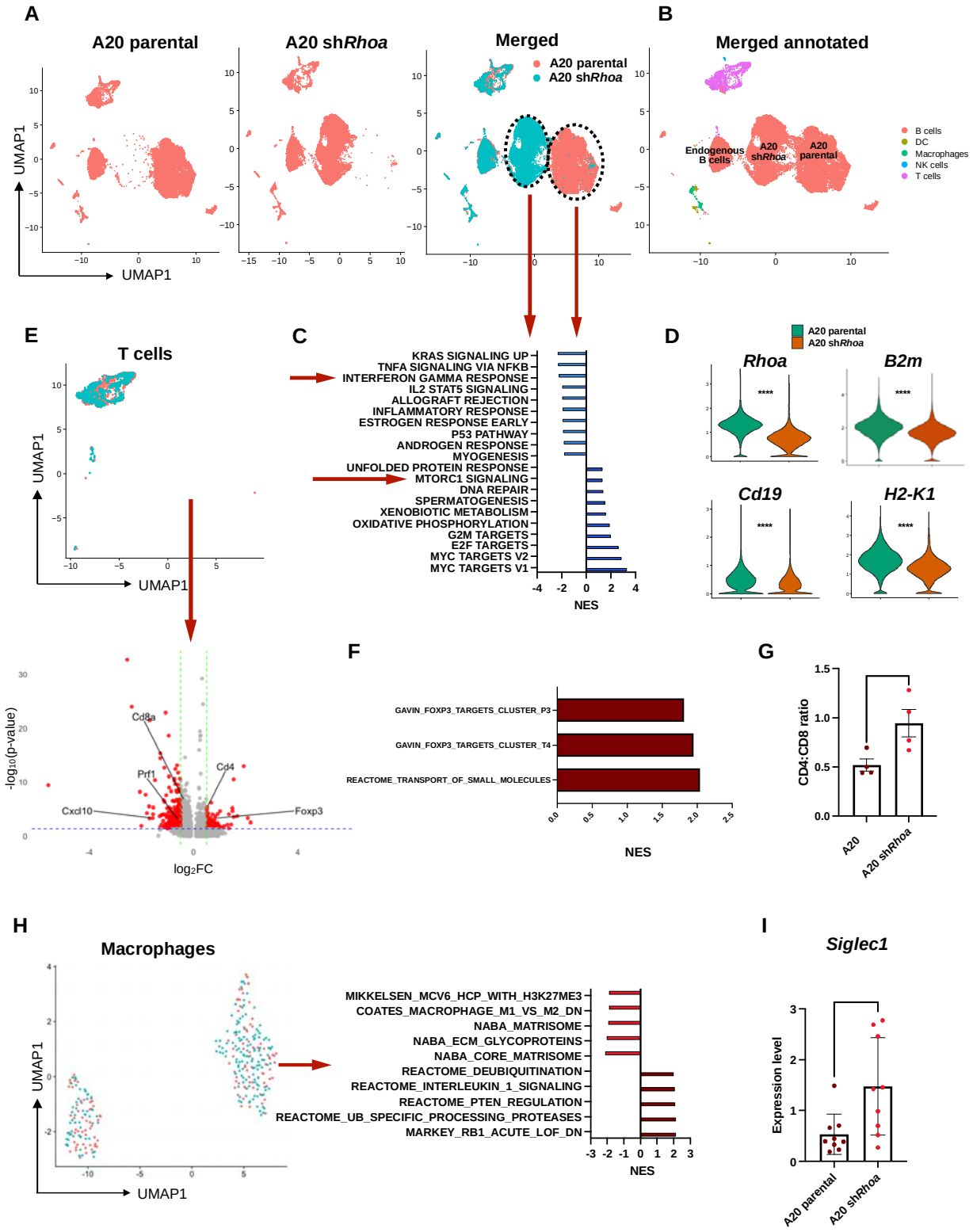
A
A20 parental
A20 shRhoa
Merged
A20 parental
A20 shRhoa
B
Merged annotated
Endogenous B cells
A20 shRhoa
A20 parental
B cells
DC
Macrophages
NK cells
T cells
UMAP1
UMAP1
E
T cells
UMAP1
UMAP1
C
KRAS SIGNALING UP
TNFA SIGNALING VIA NFKB
INTERFERON GAMMA RESPONSE
IL2 STAT5 SIGNALING
ALLOGRAFT REJECTION
INFLAMMATORY RESPONSE
ESTROGEN RESPONSE EARLY
P53 PATHWAY
ANDROGEN RESPONSE
MYOGENESIS
UNFOLDED PROTEIN RESPONSE
MTORC1 SIGNALING
DNA REPAIR
SPERMATOGENESIS
XENOBIOTIC METABOLISM
OXIDATIVE PHOSPHORYLATION
G2M TARGETS
E2F TARGETS
MYC TARGETS V2
MYC TARGETS V1
NES
D
A20 parental
A20 shRhoa
Rhoa
B2m
Cd19
H2-K1
****
-log10(p-value)
log2FC
Cd8a
Prf1
Cd4
Cxcl10
Foxp3
F
GAVIN_FOXP3_TARGETS_CLUSTER_P3
GAVIN_FOXP3_TARGETS_CLUSTER_T4
REACTOME_TRANSPORT_OF_SMALL_MOLECULES
NES
G
CD4:CD8 ratio
A20
A20 shRhoa
H
Macrophages
UMAP1
UMAP1
MIKKELSEN_MCV6_HCP_WITH_H3K27ME3
COATES_MACROPHAGE_M1_VS_M2_DN
NABA_MATRISOME
NABA_ECM_GLYCOPROTEINS
NABA_CORE_MATRISOME
REACTOME_DEUBIQUITINATION
REACTOME_INTERLEUKIN_1_SIGNALING
REACTOME_PTEN_REGULATION
REACTOME_UB_SPECIFIC_PROCESSING_PROTEASES
MARKEY_RB1_ACUTE_LOF_DN
NES
I
Siglec1
Expression level
A20 parental
A20 shRhoa

Figure 4: RHOA loss fosters immunosuppressive lymphoma microenvironments

A) UMAP plots of A20 parental, A20 sh*Rhoa*, and merged data sets from in vivo lymphoma tumors (n = 4 tumors per genotype). **B)** Annotated cell types within merged data. **C)** GSEA depicting top 10 upregulated and downregulated gene sets in A20 sh*Rhoa* tumors compared to A20 parental tumors. **D)** Violin plot of *Rhoa*, *Cd19, B2m*, and *H2-K1* normalized expression in A20 parental and A20 sh*Rhoa* tumors ($-\log_2FC = -0.5$). **E)** Volcano plot representing differentially expressed genes between T cells within A20 parental and A20 sh*Rhoa* LMEs ($\log_2FC>|0.5|$, $p<0.05$). **F)** GSEA of bulk annotated T cells from A20 shRhoa tumors compared to A20 parental tumors. **G)** CD4:CD8 ratio of annotated T cells. **H)** GSEA depicting top 5 upregulated and downregulated gene sets in annotated macrophages of A20 sh*Rhoa* LMEs compared to macrophages in A20 parental LMEs. **I)** *Siglec1* expression of macrophages in parental or sh*Rhoa* LMEs ($\log_2FC=1.98$, $p=0.459$). NES - normalized enrichment score. G and I analyzed with Student's T-test and represent of mean ± SEM of 4 tumor samples per genotype. (* $p<0.05$)

559 **FIGURE 5**

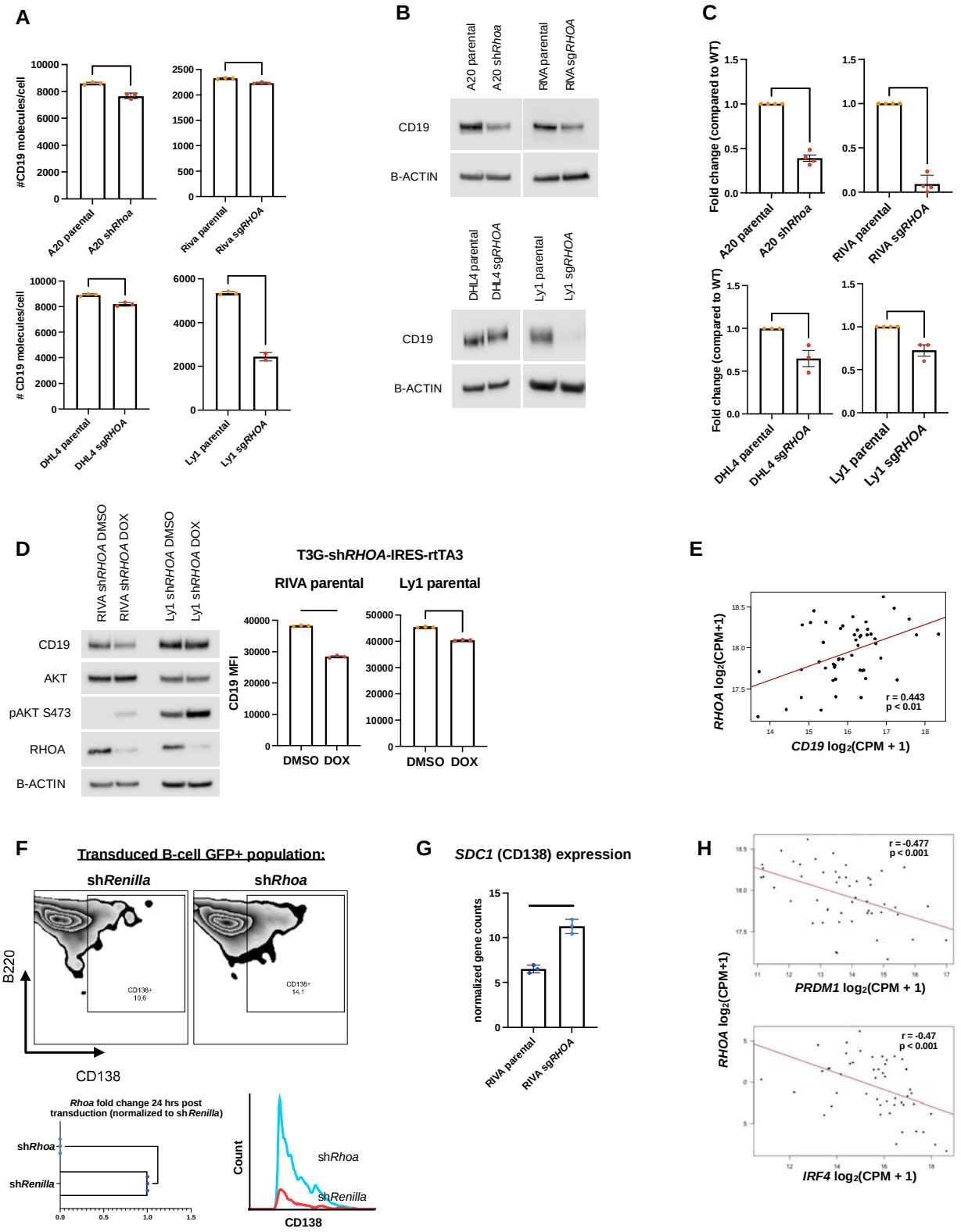

560

Figure 5: CD19 surface density is reduced in RHOA LoF systems. A) Phycoerythrin fluorescence quantitation flow cytometry revealing CD19 molecules per cell in RHOA LoF lines. **B)** Western blot of bulk CD19 protein levels in RHOA LoF cells **C.** Transcript levels of *CD19*/*Cd19* in RHOA LoF cells. **D.** Western blot and flow cytometry of RIVA and Ly1 inducible sh*RHOA* knockdown after 10 days of doxycycline (1 µg/mL) exposure. **E)** Correlation between *RHOA* and *CD19* in PCAWG data. **F)** Flow cytometry analysis of murine B cells after stimulating and transducing with sh*Rhoa* or sh*Renilla* or 72 h. Top, viable, GFP+ B220+ CD138+ cells. Bottom left, qPCR of *Rhoa* transcripts 24 h after transduction. Bottom right, histogram of CD138+ cells). **G)** Normalized gene counts (CPM) of *SDC1* in RIVA RNA-seq data. **H)** Correlation of *RHOA* and *PRDM1* and *IRF4* in PCAWG data set. r = Spearman's correlation coefficient. Statistical comparisons of WT and sg/sh*RHOA* in A,C,D,F,G performed using Student's T-test and represent mean ± SEM of 2-4 independent experiments. CPM - counts per million (* $p<0.05$ ** $p<0.01$ *** $p<0.001$ **** $p<0.0001$)

575 **FIGURE 6**

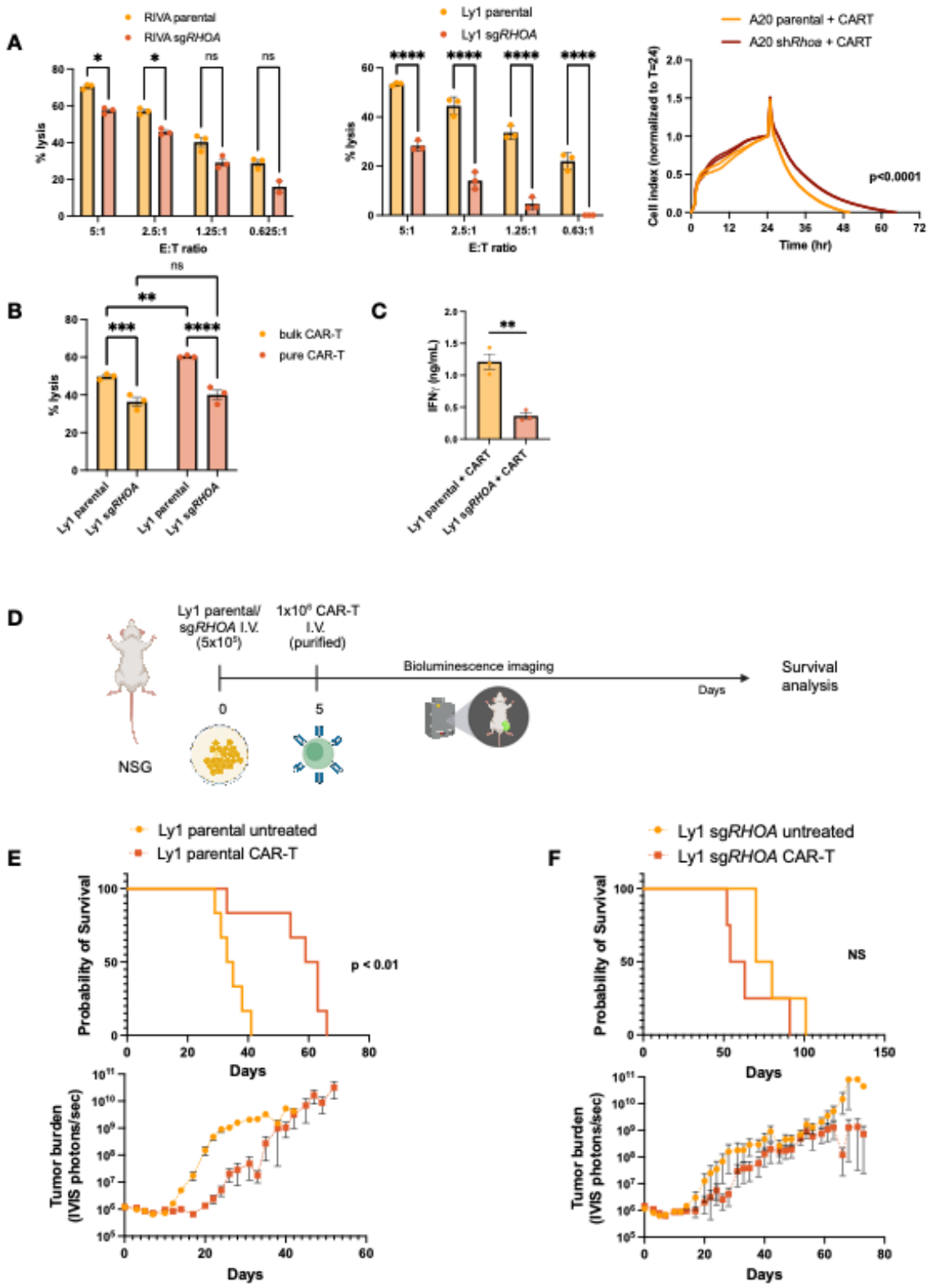

576

Figure 6: CAR-19 killing is reduced in RHOA LoF lymphomas. A) Left and middle, flow cytometry cytotoxicity assay of RIVA and Ly1 WT and RHOA LoF cells cocultured with purified 4-1BB costimulated CD19-CAR-T cells for 6 h. % lysis = 1 - (# targets remaining after coculture/# targets alone). Right, xCELLigence impedance assay of A20 parental or sh*Rhoa* cells with bulk transduced m1928z CAR-T cells (E:T=3:1, CAR-Ts added at 24h, p-value via 2-way ANOVA, data reflects 2 independent experiments). **B)** Luminescence-based cytotoxicity assay of Ly1 WT and RHOA LoF cells cocultured with bulk transduced or purified CD28 costimulated CD19 CAR-T cells for 18 h at 2:1 E:T. P-value derived via 2-way ANOVA. **C)** ELISA of IFNγ in supernatants from the cocultures with purified CAR-T cells in **B**. **D**) Schematic of in vivo CAR-T efficacy with Ly1 RHOA LoF system. **E-F.** Survival curve and tumor burden measurements of Ly1 parental untreated (n=6), Ly1 parental 1M CAR-T treated (n=6), Ly1 sg*RHOA* untreated (n=4), Ly1 sgRHOA 1M CAR-T treated (n=6). P-value determined via Log-rank test. Significance determined in A and B via 2-way ANOVA, and C via Student's T-test. All panels reflect mean ± SEM of 3 independent experiments unless otherwise stated. (* $p<0.05$ ** $p<0.01$ *** $p<0.001$ **** $p<0.0001$)

METHODS

Ethics Statement

The animal experiments were conducted with strict adherence to the institutional guidelines at the University of Miami Miller School of Medicine and follow faithfully the standards of the Institutional Animal Care and Use Committee (IACUC). The Cancer Modeling Shared Resource (CMSR) at the Sylvester Comprehensive Cancer Institute of the University of Miami Miller School of Medicine agree fully to these standards for the entirety of the study involving mice under protocol 21-103 -ad06.

Mice and cell Lines

NOD.Cg-*Prkdc*^{scid} *Il2rg*^{tm1Wjl}/SzJ (NSG) mice 6-8 weeks of age were used to create the xenogeneic OCI-Ly1 parental and OCI-Ly1 sg*RHOA* model of lymphoma. Equal numbers of male and female mice were randomized into the untreated and CAR-T treated conditions. BALB/c mice 6-8 weeks of age were used to create the A20 syngeneic model of RHOA-deficient lymphoma. Wild-type C57BL/6J mice were used and sacrificed for spleen harvest of naïve B cell populations for the ex vivo B cell plasmablast formation experiment.

All cell lines were routinely verified by STR fingerprinting and confirmed mycoplasma negative. RIVA, SU-DHL4, and A20 were cultured in complete RPMI (Fisher Scientific) - (10% FBS (VWR), 1% penicillin/streptomycin (10,000 units/mL, Fisher Scientific), and Plasmocin prophylactic (100 mg, Invivogen). OCI-Ly1 was cultured in complete IMDM (Fisher Scientific) – (20% FBS (VWR), 1% penicillin/streptomycin (10,000 units/mL, Fisher Scientific), and Plasmocin prophylactic (100 mg, Invivogen). Cell lines were purchased by American Type Culture Collection (ATCC), Manassas, VA, USA, RIVA was purchased from DSMZ. Cells were maintained at 37 °C in a 5% CO2 humidified incubator.

RHOA LoF Engineered Cell Lines

CRISPR/Cas9 editing of parental RIVA, Ly1, and DHL4 cells to create RHOA LoF was performed via transient co-nucleofection (Lonza Nucleofector Kit V, VCA-1003) of eSpCas9(1.1)-T2A-GFP-GlntRNA or eSpCas9(1.1)-T2A-mCherry-GlntRNA cloned with sgRNAs targeting exon 2 (TCCGGAAGAAACTGGTGATT) and exon 3 (GATACCGATGTTATACTGAT) of *RHOA* for 24 h followed by FACS sorting of double-positive single cells in 96-well plates. Candidates were expanded and assessed for RHOA LoF via active Rho pulldown assay.

To generate inducible human *RHOA* knockdown systems a 97mer targeting *RHOA* was designed (TGCTGTTGACAGTGAGCGACTGTAACTACTTTATAACTAATAGTGAAGCCACAGATGTATTAGTTATAAAGTAGTTACAGCTGCCTACTGCCTCGGA), PCR amplified with XhoI and EcoRI restriction sites and cloned into the Tet-ON miR-E (miR-30 variant)-based RNAi vector, LT3GEPIR, as previously described.[62] Lentiviral particles were produced as described below and used to transduce RIVA and Ly1 cells. Cells were selected with puromycin (1µg/mL) and cultured for 2-3 passages (10 days) in doxycycline (1 µg/mL). This duration of induction revealed knockdown of bulk RHOA on Western blot and was used for subsequent experiments.

To create RHOA rescue cell lines we engineered the human CRISPR/Cas9 RHOA LoF systems described above via lentiviral introduction of RHOA CDS expression. RHOA ORF GFP-tagged lentiviral particles were purchased (Origene, RC203303L2V) and used to infect cells at MOI > 0.5:1. GFP+ cells were sorted, expanded, and validated for RHOA rescue with active Rho pulldown assay.

Stable knockdown of *Rhoa* in murine A20 lymphoma cells was conducted by designing a 97mer targeting *Rhoa* (TGCTGTTGACAGTGAGCGATGGGTATTCAGTTTTTTGAAATAGTGAAGCCACAGATGTATTTCAAAAAACTGAATACCCACTGCCTACTGCCTCGGA), PCR amplifying with XhoI and EcoRI restriction sites, and cloning into the mirE-based retroviral shRNA expression vector MLS-E, as

644 previously described.[62] GFP+ cells were sorted, expanded, and validated for *Rhoa* knockdown
645 via active Rho pulldown assay.
646
647 **Tumor models and T cell adoptive transfer**
648 The syngeneic RHOA-deficient model of lymphoma was generated by irradiating 6-12 week
649 BALB/c recipients with 3.5 Gy TBI the morning of lymphoma cell injections. $1x10^6$ A20-luc
650 parental and A20-luc sh*Rhoa* cells were then injected via tail-vein and monitored with IVIS
651 imaging biweekly. Mice were sacrificed near endpoint and liver-engrafted tumors were
652 harvested for scRNA-seq analyses.
653 The in vivo CAR-T efficacy experiment was conducted by
654 engrafting 24 NSG mice 6-12 weeks old with $5x10^5$ luciferase labeled Ly1 parental or Ly1
655 sg*RHOA* cells. Five days later, on day 10 of pSLCAR-CD19-28z CAR-T production and two
656 days after sorting GFP+ cells, purified human CAR-Ts were injected at a dose of $1x10^6$ per
657 mouse. Mice were monitored and imaged with IVIS every 2-3 days.
658
659 **CAR-T cell generation**
660 Human – The pSLCAR-CD19-28z 2nd generation CAR construct used to generate CD28
661 costimulated CD19-directed human CAR-T cells has been previously characterized.[63] For CAR
662 engineering, CD3+ cells were enriched with the EasySep Negative Human T cell Kit (StemCell,
663 19051) using PBMCs from a single donor (StemCell, 70025.1). Cells were activated with
664 CD3/CD28 Dynabeads (1:1 cell to bead ratio) (Thermo Fisher, 11131D) and cultured in CTS
665 OpTmizer T cell expansion media (5% human AB serum, 100 IU/mL P/S) with 100 IU/mL
666 human IL-2, 10 ng/mL human IL-7 (StemCell, 78196), and 10 ng/mL human IL-15 (StemCell,
667 78218). After 48 h, cells were transduced with pSLCAR-CD19-28z lentiviral particles seeded
668 onto a retronectin-coated plate at MOI = 27. Fresh media was added the following day. 48-96 h
669 after transduction cells were either GFP+ sorted or used as bulk cultures in cytotoxic assays.

CAR-Ts were never used in experiments beyond 12 days of culturing. For some assays, a 4-1BB costimulated CD19-directed CAR-T was used (BPS Bioscience, #78171) and cultured in RPMI (10% FBS, 100 IU/mL P/S) and human IL-2 (10 IU/mL, R&D 202-IL-050/CF).

Mouse - For murine CAR-19 generation, spleens from 6-12 week BALB/c mice were prepared as single-cell suspensions and lysed with ACK lysis (Thermo Fisher, A1049201) for 4 min. T cells were then isolated with EasySep Mouse T Cell Isolation Kit (StemCell, 19851A), activated with mouse CD3/CD28 Dynabeads (Thermo Fisher, 11452D), and cultured in mRPMI with human IL-2 (80 IU/mL). The next day, previously prepared SFG-m1928z[64] - mCherry retroviral particles were seeded onto a retronectin-coated plate after which T cells were added at $2x10^6$ cells/well and spinfected for 10 min at 1800 RPM at 32 °C. Media was added the following day and bulk transduced m1928z CAR-T cells (~70-80% mCherry+) cells were used in cytotoxic assays.

Whole genome sequencing analysis

Raw FASTQ from tumor and normal paired samples were aligned against the GRCh38 genome build and somatic single-nucleotide variants (SNVs), short insertion-deletions variants (INDELs), copy-number variants (CNVs) and structural variants (SVs) were called using the MGP1000 Pipeline. We performed additional quality filters as previously described.[9] We applied the dN/dScv method to detect genes under positive selection in r/r. The mutational signature analysis of single-base substitutions (SBSs) was performed as described previously. Complex events, such as chromothripsis, chromoplexy, and templated insertions, were defined after manual inspection, as previously described.[9]

RNAseq analysis and Gene Set Enrichment Analysis

The raw count data was filtered to remove genes with less than 10 reads in greater than 95% of samples. The trimmed mean of M-values (TMM) normalization was applied. This method

estimates a scale factor used to reduce technical bias between samples with different library sizes. We used the DESeq2 (Fig. 1) or EdgeR (cell line RNA-seq data) R package to implement the differential expression analysis. P values were corrected for multiple testing using Benjamini-Hochberg false discovery rate method and only genes with FDR<0.05 were considered. The Gene Set Enrichment Analysis (GSEA) was performed using the fgsea R package. The Hallmark gene sets collection, retrieved from MSigDB database v7.4 (8), was enriched with two INF signatures, ISG.RS and IFNG.GS, previously described to be associated with response to immunotherapy.[65] Genes were ranked using the statistic derived from differential expression analysis. Gene collections for the T-cell and Macrophage GSEA (Fig. 4) came from mouse MSigDB collection M2 and all genes were preranked with FDR<0.05, p<0.05, and $Log_2FC>|0.5|$.

Single-cell RNA-sequencing

A20 tumors engrafted in syngeneic BALB/c recipients were harvested as liver nodules near endpoint and prepared as single-cell suspensions for the 10x Chromium platform. Briefly, cells were partitioned into nanoliter gel beads-in-emulsion (GEMs). A pool of ~3,500,000 10x Genomics barcodes were used to separately and uniquely index each individual cell. Libraries were then created and sequenced on the Illumina Novaseq X, with 10x barcodes used to assign reads back to individual partitions, and therefore, to each individual cell. 6,000 cells per sample were targeted with 50K reads per cell. The raw data was processed and barcoded using Cell Ranger (10x Genomics). Cells with > 500 RNA molecules, > 250 genes, and < 20% mitochondrial genes were filtered for analysis resulting in samples with a median of 4,441 cells (range 3334-4878). The Seurat package (v.5.1.0) was used to create objects and normalize, scale, and dimensionally reduce data, as well as to find clusters and compute variable features between them. The SingleR package (v.2.4.1) was used to annotate cells by calling immgen

library. The FindMarkers function using min.pct=0.10 (macrophages) or 0.05 (T cells) was used to determine differentially expressed genes.

Active Rho pulldown assay and western blotting

WT and RHOA LoF cells were passaged and seeded at equal densities in 150 mm tissue culture dishes 48 h before creating protein lysates. At least 250 µg of lysate was subject to treatment with GST-Rhotekin as described by manufacturer (Thermo Scientific, 16116) and subject to GST-Rhotekin pulldown and Western blot analysis.

Antibodies used for western blotting include: GAPDH (D16H11) XP® Rabbit mAb (Cell Signaling, Cat# 5174), Cyclophilin B Polyclonal Antibody (Thermo Fisher, Cat# PA1-027A), RhoA (67B9) Rabbit mAb (Cell Signaling Cat# 2117), Akt (pan) (11E7) Rabbit mAb (Cell Signaling, Cat# 4685), Phospho-Akt (Ser473) (193H12) Rabbit mAb (Cell Signaling, Cat# 4058), Stat1 Antibody (Cell Signaling, Cat# 9172), Phospho-Stat1 (Tyr701) (58D6) Rabbit mAb (Cell Signaling, Cat# 9167), CD19 (Intracellular Domain) (D4V4B) XP® Rabbit mAb (Cell Signaling, Cat# 90176), IRF-1 (D5E4) XP® Rabbit mAb (Cell Signaling, Cat# 8478).

Transwell migration Assay

WT and RHOA LoF cells were passaged at equal numbers the day before and then seeded at a density of $1x10^6$ in 300 µL on the top chamber of a 5-micron chamber (Sterlitech, 9315012) in serum free RPMI. The bottom chamber contained serum free RPMI + SDF-1 (CXCL12) (300 ng/mL, R&D) in a total volume of 1 mL. After 4 h, the filter was carefully removed and the bottom chamber containing migrated cells was analyzed via flow cytometry. The total events collected in 500 µL were recorded and analyzed.

Drug treatment assay

Idelalisib, capivasertib, and rapamycin (MedChemExpress) were serially diluted 10 times in 25 µL of growth media with DMSO vehicle in a 384-well plate, in quadruplicates. An equal volume containing 2,500 cells was added and allowed to incubate with drug for 72 h. CellTiter-Glo® reagent (Promega, G7570) was then added to assess viability via luminescence.

Drug sensitivity correlation with *RHOA* expression

The DepMap data explorer (depmap.org) was accessed and a custom analysis with the Pearson correlation, Sanger GDSC1 data set, *RHOA*, and a curated cell line list was run. The cell lines were pulled from the disease subtype: DLBCL- NOS, ACTIVATED B-CELL LIKE, GERMINAL CENTER B-CELL LIKE. Raw data was downloaded and plotted, and correlations analyzed via Pearson's correlation coefficient.

ELISA

CXCL10 - cells were seeded at equal densities ($5x10^5$ cells/mL) in triplicates and supernatants were collected 48 h later. 25 µL of supernatant was then used in the Human IP-10 ELISA Kit (Abcam, ab173194). IFNγ - 25 µL of supernatant was collected after 18 h cocultures (see Cytotoxicity Assay) and used in the Human IFN gamma ELISA Kit Abcam, ab174443). Quantification was calculated using standard curve and per manufacture's protocol.

IFNγ treatments

To assess transcriptional and membrane level responses to IFNγ treatment, cells were seeded at 500,000 cells/mL and treated with IFNγ (30 ng/mL, MedChemExpress Cat# HY-P7025, Cat# HY-P7071) for 2 h or 48 h, respectively. RNA was harvested for qPCR analysis and cells for flow cytometry. To assess restoration of IFNγ response, cells were seeded at 500,000 cells/mL and treated with DMSO or idelalisib (1 µM) for 24 h. IFNγ (30 ng/mL) was then added to the culture for 2 h and then proteins were isolated for Western blot analysis.

CD19 membrane quantitation

The BD Quantibrite™ PE Phycoerythrin Fluorescence Quantitation Kit was used to calculate the number of CD19 molecules on WT and RHOA LoF cells. Briefly, Quantibrite PE tubes contain beads with known quantities of PE molecules conjugated. By running these at the same time and conditions as experimental samples stained with CD19-PE (BD, 555413), and using the lot specified PE molecules/bead, we converted PE molecules/cell to antibodies/cell, corresponding to number of CD19 molecules/cell. 100,000 cells per sample were prepared for analysis by washing 1x with FACS buffer before incubating with CD19-PE for 25 min.

Flow cytometry

Standard flow cytometry of analysis of isogenic cells was conducted by washing cells ($1e^5$-$5e^5$ cells/sample) with 1mL FACS buffer (Thermo, 00-4222-26) before incubating with Fc receptor blocking cocktails (human, Thermo Fisher 14-9161-73 (2.5 µL/sample), mouse, BD 553141 (1 µL/sample). After 5-15 min. of blocking, antibodies were added at standard manufacturer concentrations. Cells were washed 2x with 1mL FACS buffer and analyzed on Attune NxT flow cytometer. Antibodies used include: PE Mouse Anti-Human CD19 (BD Biosciences, Cat# 555413), PE-Cy™7 Rat Anti-Mouse CD19 (BD Biosciences, Cat# 561739), PerCP/Cyanine5.5 Anti-Mouse CD3 (BioLegend, Cat# 100218), PE/Cyanine7 Anti-Mouse β2-microglobulin (BioLegend, Cat# 154508), FITC Anti-Human β2-microglobulin (BioLegend, Cat# 316304), PE/Cyanine7 Anti-Human HLA-A,B,C (BioLegend, Cat# 311430).

Flow cytometry analysis of viably frozen ex vivo A20 lymphoma tumors was conducted by thawing and removing dead cells with EasySep Dead Cell Removal (Annexin V) Kit (StemCell, 17899). Tumor B-cells were depleted with EasySep Mouse CD19 Positive Selection Kit II (StemCell, 18954) and remaining cells were subject to flow cytometry staining protocols after

blocking with anti-CD16/CD32 Fc block (BD, 553142) using the following reagents: Live/Dead Fixable Red (Thermo, L34971) and anti-CD3 PerCP/Cy5.5 (Biolegend, 100218)

qRT-PCR

First-strand cDNA synthesis was performed using Oligo (dT) primer and SuperScript III RT (Thermo Fisher, AM5730G, 18080044), according to the manufacturer's protocols. qRT-PCR was performed using a StepOnePlusTM Real-Time PCR System (ThermoFisher Scientific). Relative changes in expression were calculated using the comparative Ct (ΔΔCt) method. 18S rRNA was measured as an internal control for changes in RNA levels. All qPCR reactions were performed using PowerUpTM SYBR® Green Master Mix (Thermo Fisher, #A25742) unless otherwise stated. Primers used include: Human *18S* - F: CAGCCACCCCGAGATTGAGCA R: TAGTAGCGACGGGCGGTGTG, Human *IRF1* - F: ACACAGGCCGATACAAAGCA R: CCATCCACGTTTGTTGGCTG, Human *STAT1* - F: TAATCAGGCTCAGTCGGGGA R: GAAGGTGCGGTCCCATAACA, Human *CD19* - F: TGGGTAATGGAGACGGGTCT R: TAGCCCTCCCCTTCCTCTTC, Mouse *Rn18S* - F: ATTCGTATTGCGCCGCTAGA R: CCCGGACATCTAAGGGCATC, Mouse Cd19 - F: TGTCAGCATGCACACATCCT R: GGACCAGGTTTCCCAGGATG, Mouse *Rhoa* F: CGTGGCTGAACTGAGAGTGT R: GCCAACTCTACCTGCTTCCC.

Mouse ex vivo B cell stimulation experiment

6-12 week wild-type C57BL/6J mice were sacrificed and B cells were isolated, stimulated, and transduced, as previously described.[44] Briefly, B cells were isolated via MagniSort™ Mouse B cell Enrichment Kit (Fisher Scientific, 8804-6827), cultured in mRPMI (10% FBS, 100 IU/mL P/S, 1x nonessential amino acids, 1 µM sodium pyruvate, 10 mM HEPES, 50 µM B-ME, 2 mM glutamine) and activated for 24 h with 10 µg/mL LPS. After 24 h, the cells were transduced with concentrated retroviral particles (100 µL) that were seeded onto a retronectin coated 6-well non-

tissue culture treated plate (see virus generation and transduction below). 48 hr after transduction B cell were stained with live/dead fixable red (Thermo Fisher, L23102), anti-B220-PE (BD, 553090) and anti-CD138-PE/Cy7 (Biolegend, 142513) and population were assessed via flow cytometry.

Virus generation and transduction

Retroviruses (m1928z, MLS-E) were generated by transfecting 293T (ATCC, CRL-3216) cells with transfer plasmid and pCL-eco helper plasmid at 3:1 ratios. Lentiviruses (pSLCAR-CD19-28z, LT3GEPIR) were generated by transfecting Lenti-X 293T (Takara, 632180) cells with 4th generation lentiviral transfer plasmids, pMDLg/pRRE, pMD.2G, and pRSV at a 3:1 ratio of transfer to helper plasmids. Briefly, 293T cells were seeded at $5e^6$ cells in 150 mm dishes. 24-36 h later, DNA was transfected using lipofectamine 3000 (Thermo Fisher L3000001). After 6 h, the transfection media was carefully replaced with fresh DMEM (10% FBS, 100 IU/mL P/S). Supernatant was harvested 48 h later and concentrated with Retro-X or Lenti-X Concentrator (Takara, 631456, 631232) into 100 µL aliquots and frozen in -80 °C for future studies. For most transductions, virus was co-localized onto non tissue culture-treated 6-well retronectin-coated (20 µg/mL, Takara) and 0.5% PBS/BSA blocked plates at 2000xg for 2 h at 32 °C.

Flow cytometry cytotoxicity assay

CAR-T cells were serially diluted in 100 µL of target cell media in triplicates in a 96-well plate. Target cells were labeled with CellTrace Yellow Cell Proliferation Kit (5 µM, Thermo Fisher, C34567), washed, and added to CAR-T containing or control wells at $1x10^4$ cells/100 µL. 6-24 h later plates were analyzed via flow cytometry, with FSC and SSC adjusted on target cells and settings to collect all events in 100 µL.

$$\%\ lysis = 1 - (\#\ target\ cells\ remaining\ in\ coculture - \#\ cells\ remaining\ in\ target\ only\ wells)$$

Impedance-based cytotoxicity assay

Xcelligence RTCA e-Plates (Agilent, 5469830001) were prepared for A20 lymphoma tethering by coating wells with 0.5 mg/mL anti-B220 overnight at 4 C. The following day wells were washed, loaded with 50 µL of target cell media analyzed on the RTCA instrument for a brief background reading. Plates were then retrieved from the incubator and A20 cells were seeded at 10,000 cells/well in 100 µL. Instrument was set to collect readings every 30 sec for 24 h, upon which murine CAR-T cells were added at various E:T ratios in 100 µL. Readings continued for 72 h and the raw data (cell index) was plotted and analyzed.

Luminescence-based cytotoxicity assay

Firefly-luciferase labeled Ly1 and Ly1 RHOA LoF cells were cocultured with bulk and purified pSLCAR-CD19-28z CAR-T cells as described in the flow cytometry cytotoxicity assay, without CellTrace labeling. 18-24 h later, plates were centrifuged and wells were washed 1x with PBS and then cocultured cells were lysed with 20 µL 1x lysis buffer (Promega, E1500) for 15 min. Plates were centrifuged and supernatant was transferred 96-well white bottom plates. 100 µL of Luciferase Assay Reagent was added to lysates and plates were immediately read on luminometer. $\%\ lysis = 1 - (luminescence\ of\ coculture - luminscence\ of\ target\ cells\ alone)$

PBMC coculture

PBMCs from the same donor as used to generate human CD28 costimulatory CAR-Ts were thawed and activated overnight. The following day they were cultured with RIVA parental and RHOA LoF cells for 40 h with E:T = 1:1 with or without an 0.5 µg/mL IFNγ neutralizing antibody (BD, 554699)

Pharmacologic RHOA inhibition and CD19 analysis

250,000 RIVA and Ly1 parental and RHOA LoF cells were seeded in 500 µL in a 24-well plate in triplicates and treated with DMSO Rho specific inhibitor Rhosin (MedChemExpress, HY-12646) at various concentrations for 24 h. Cells were then subject to flow analysis after Fc block and staining with anti-CD19 (BD, 555413) at manufacturer recommendation centration.

QUANTIFICATION AND STATISTICAL ANALYSIS

All statistical analyses of transwell migration data, cell viability data, flow cytometry data, qPCR data, drug sensitivity data, ELISA data, cytotoxicity assay data, and mouse survival data were conducted in Prism GraphPad software. WGS, RNA-seq, and scRNA-seq data were analyzed within the R framework using the statistical methods stated above.

REFERENCES:

1. Neelapu, S. S. *et al.* Five-year follow-up of ZUMA-1 supports the curative potential of axicabtagene ciloleucel in refractory large B-cell lymphoma. *Blood* **141**, 2307–2315 (2023).
2. Bachy, E. *et al.* A real-world comparison of tisagenlecleucel and axicabtagene ciloleucel CAR T cells in relapsed or refractory diffuse large B cell lymphoma. *Nat Med* (2022) doi:10.1038/s41591-022-01969-y.
3. Jain, M. D. *et al.* Five-Year Follow-Up of Standard-of-Care Axicabtagene Ciloleucel for Large B-Cell Lymphoma: Results From the US Lymphoma CAR T Consortium. *JCO* **42**, 3581–3592 (2024).
4. Locke, F. L. *et al.* Axicabtagene Ciloleucel as Second-Line Therapy for Large B-Cell Lymphoma. *N Engl J Med* **386**, 640–654 (2022).

898 5. Deng, Q. *et al.* Characteristics of anti-CD19 CAR T cell infusion products associated with
899 efficacy and toxicity in patients with large B cell lymphomas. *Nat Med* **26**, 1878–1887
900 (2020).
901 6. Scholler, N. *et al.* Tumor immune contexture is a determinant of anti-CD19 CAR T cell efficacy
902 in large B cell lymphoma. *Nat Med* **28**, 1872–1882 (2022).
903 7. Jain, M. D. *et al.* Tumor interferon signaling and suppressive myeloid cells are associated with
904 CAR T-cell failure in large B-cell lymphoma. *Blood* **137**, 2621–2633 (2021).
905 8. Chen, P.-H. *et al.* Activation of CAR and non-CAR T cells within the tumor microenvironment
906 following CAR T cell therapy. *JCI Insight* **5**, e134612 (2020).
907 9. Jain, M. D. *et al.* Whole-genome sequencing reveals complex genomic features underlying
908 anti-CD19 CAR T-cell treatment failures in lymphoma. *Blood* blood.2021015008 (2022)
909 doi:10.1182/blood.2021015008.
910 10. Cherng, H.-J. J. *et al.* Risk assessment with low-pass whole-genome sequencing of cell-free
911 DNA before CD19 CAR T-cell therapy for large B-cell lymphoma. *Blood* **140**, 504–515 (2022).
912 11. Shouval, R. *et al.* Impact of TP53 Genomic Alterations in Large B-Cell Lymphoma Treated
913 With CD19-Chimeric Antigen Receptor T-Cell Therapy. *JCO* JCO.21.02143 (2021)
914 doi:10.1200/JCO.21.02143.
915 12. Sworder, B. J. *et al.* Determinants of resistance to engineered T cell therapies targeting
916 CD19 in large B cell lymphomas. *Cancer Cell* **41**, 210-225.e5 (2023).
917 13. Isshiki, Y. *et al.* EZH2 inhibition enhances T cell immunotherapies by inducing lymphoma
918 immunogenicity and improving T cell function. *Cancer Cell* **0**, (2024).

919 14. Upadhyay, R. *et al.* A Critical Role for Fas-Mediated Off-Target Tumor Killing in T-cell
920 Immunotherapy. *Cancer Discovery* **11**, 599–613 (2021).
921 15. Chapuy, B. *et al.* DLB*class*: A Probabilistic Molecular Classifier to Guide Clinical Investigation
922 and Practice in Diffuse Large B-Cell Lymphoma. *Blood* (2024)
923 doi:10.1182/blood.2024025652.
924 16. Chapuy, B. *et al.* Molecular subtypes of diffuse large B cell lymphoma are associated with
925 distinct pathogenic mechanisms and outcomes. *Nat Med* **24**, 679–690 (2018).
926 17. Monti, S. *et al.* Integrative Analysis Reveals an Outcome-Associated and Targetable Pattern
927 of p53 and Cell Cycle Deregulation in Diffuse Large B Cell Lymphoma. *Cancer Cell* **22**, 359–
928 372 (2012).
929 18. Muppidi, J. R. *et al.* Loss of signalling via Gα13 in germinal centre B-cell-derived lymphoma.
930 *Nature* **516**, 254–258 (2014).
931 19. Jiang, X. *et al.* HGAL, a germinal center specific protein, decreases lymphoma cell motility by
932 modulation of the RhoA signaling pathway. *Blood* **116**, 5217–5227 (2010).
933 20. Sahasrabuddhe, A. A. *et al.* The FBXO45-GEF-H1 axis controls germinal center formation and
934 B-cell lymphomagenesis. *Cancer Discovery* (2025) doi:10.1158/2159-8290.CD-24-0442.
935 21. Reddy, A. *et al.* Genetic and Functional Drivers of Diffuse Large B Cell Lymphoma. *Cell* **171**,
936 481-494.e15 (2017).
937 22. Aaltonen, L. A. *et al.* Pan-cancer analysis of whole genomes. *Nature* **578**, 82–93 (2020).
938 23. Simón-Carrasco, L., Pietrini, E. & López-Contreras, A. J. Integrated analysis of FHIT gene
939 alterations in cancer. *Cell Cycle* **23**, 92–113 (2024).

940 24. Wright, G. W. *et al.* A Probabilistic Classification Tool for Genetic Subtypes of Diffuse Large B
941 Cell Lymphoma with Therapeutic Implications. *Cancer Cell* **37**, 551-568.e14 (2020).
942 25. DepMap. DepMap 24Q4 Public. Figshare+. Dataset.
943 https://doi.org/10.25452/figshare.plus.27993248.v1 (2024).
944 26. Fujisawa, K., Fujita, A., Ishizaki, T., Saito, Y. & Narumiya, S. Identification of the Rho-binding
945 Domain of p160ROCK, a Rho-associated Coiled-coil Containing Protein Kinase *. *Journal of*
946 *Biological Chemistry* **271**, 23022–23028 (1996).
947 27. Vazquez, F., Ramaswamy, S., Nakamura, N. & Sellers, W. R. Phosphorylation of the PTEN Tail
948 Regulates Protein Stability and Function. *Mol Cell Biol* **20**, 5010–5018 (2000).
949 28. Kumagai, S. *et al.* An Oncogenic Alteration Creates a Microenvironment that Promotes
950 Tumor Progression by Conferring a Metabolic Advantage to Regulatory T Cells. *Immunity*
951 **53**, 187-203.e8 (2020).
952 29. Girdlestone, J., Isamat, M., Gewert, D. & Milstein, C. Transcriptional Regulation of HLA-A
953 and -B: Differential Binding of Members of the Rel and IRF Families of Transcription Factors.
954 *Proceedings of the National Academy of Sciences of the United States of America* **90**,
955 11568–11572 (1993).
956 30. Purbey, P. K. *et al.* Opposing tumor-cell-intrinsic and -extrinsic roles of the IRF1
957 transcription factor in antitumor immunity. *Cell Reports* **43**, (2024).
958 31. Gobin, S. J. P., Biesta, P. & Van den Elsen, P. J. Regulation of human beta 2-microglobulin
959 transactivation in hematopoietic cells. *Blood* **101**, 3058–3064 (2003).

960 32. Harikumar, K. B. *et al.* K63-linked polyubiquitination of transcription factor IRF1 is essential
961 for IL-1-induced production of chemokines CXCL10 and CCL5. *Nat Immunol* **15**, 231–238
962 (2014).
963 33. Forero, A. *et al.* Differential Activation of the Transcription Factor IRF1 Underlies the
964 Distinct Immune Responses Elicited by Type I and Type III Interferons. *Immunity* **51**, 451-
965 464.e6 (2019).
966 34. Tsai, C.-C. *et al.* Glycogen Synthase Kinase-3β Facilitates IFN-γ-Induced STAT1 Activation by
967 Regulating Src Homology-2 Domain-Containing Phosphatase 21. *The Journal of Immunology*
968 **183**, 856–864 (2009).
969 35. Cross, D. A., Alessi, D. R., Cohen, P., Andjelkovich, M. & Hemmings, B. A. Inhibition of
970 glycogen synthase kinase-3 by insulin mediated by protein kinase B. *Nature* **378**, 785–789
971 (1995).
972 36. Fangazio, M. *et al.* Genetic mechanisms of HLA-I loss and immune escape in diffuse large B
973 cell lymphoma. *Proc Natl Acad Sci U S A* **118**, e2104504118 (2021).
974 37. Boulch, M. *et al.* Tumor-intrinsic sensitivity to the pro-apoptotic effects of IFN-γ is a major
975 determinant of CD4+ CAR T-cell antitumor activity. *Nat Cancer* **4**, 968–983 (2023).
976 38. Hori, S., Nomura, T. & Sakaguchi, S. Control of regulatory T cell development by the
977 transcription factor Foxp3. *Science* **299**, 1057–1061 (2003).
978 39. Zumwalt, T. J., Arnold, M., Goel, A. & Boland, C. R. Active secretion of CXCL10 and CCL5
979 from colorectal cancer microenvironments associates with GranzymeB+ CD8+ T-cell
980 infiltration. *Oncotarget* **6**, 2981–2991 (2014).

981 40. Pandey, V. *et al.* CXCL10/CXCR3 signaling contributes to an inflammatory microenvironment
982 and its blockade enhances progression of murine pancreatic precancerous lesions. *eLife* **10**,
983 e60646 (2021).
984 41. Spiegel, J. Y. *et al.* CAR T cells with dual targeting of CD19 and CD22 in adult patients with
985 recurrent or refractory B cell malignancies: a phase 1 trial. *Nat Med* **27**, 1419–1431 (2021).
986 42. Chen, Z. *et al.* YTHDF2 promotes ATP synthesis and immune evasion in B cell malignancies.
987 *Cell* **0**, (2024).
988 43. Healy, J. A. *et al.* GNA13 loss in germinal center B cells leads to impaired apoptosis and
989 promotes lymphoma in vivo. *Blood* **127**, 2723–2731 (2016).
990 44. He, Y. *et al.* P2RY8 variants in lupus patients uncover a role for the receptor in
991 immunological tolerance. *J Exp Med* **219**, e20211004 (2021).
992 45. Tellier, J. *et al.* Blimp-1 controls plasma cell function through the regulation of
993 immunoglobulin secretion and the unfolded protein response. *Nat Immunol* **17**, 323–330
994 (2016).
995 46. Roddie, C. *et al.* Dual targeting of CD19 and CD22 with bicistronic CAR-T cells in patients
996 with relapsed/refractory large B-cell lymphoma. *Blood* **141**, 2470–2482 (2023).
997 47. Larson, S. M. *et al.* CD19/CD20 Bispecific Chimeric Antigen Receptor (CAR) in
998 Naive/Memory T Cells for the Treatment of Relapsed or Refractory Non-Hodgkin
999 Lymphoma. *Cancer Discov* **13**, 580–597 (2023).
1000 48. Funk, C. R. *et al.* PI3Kδ/γ inhibition promotes human CART cell epigenetic and metabolic
1001 reprogramming to enhance antitumor cytotoxicity. *Blood* **139**, 523–537 (2022).

1002 49. Dickinson, M. J. *et al.* A Novel Autologous CAR-T Therapy, YTB323, with Preserved T-cell
1003 Stemness Shows Enhanced CAR T-cell Efficacy in Preclinical and Early Clinical Development.
1004 *Cancer Discov* **13**, 1982–1997 (2023).
1005 50. Jin, Z. *et al.* Lenalidomide overcomes the resistance to third-generation CD19-CAR-T cell
1006 therapy in preclinical models of diffuse large B-cell lymphoma. *Cell Oncol.* **46**, 1143–1157
1007 (2023).
1008 51. Luo, W. *et al.* Bruton tyrosine kinase inhibitors preserve anti-CD19 chimeric antigen
1009 receptor T-cell functionality and reprogram tumor micro-environment in B-cell lymphoma.
1010 *Cytotherapy* **25**, 739–749 (2023).
1011 52. Boulch, M. *et al.* A cross-talk between CAR T cell subsets and the tumor microenvironment
1012 is essential for sustained cytotoxic activity. *Science Immunology* **6**, eabd4344 (2021).
1013 53. Alizadeh, D. *et al.* IFNγ Is Critical for CAR T Cell-Mediated Myeloid Activation and Induction
1014 of Endogenous Immunity. *Cancer Discov* **11**, 2248–2265 (2021).
1015 54. Wang, W. *et al.* CD8+ T cells regulate tumour ferroptosis during cancer immunotherapy.
1016 *Nature* **569**, 270–274 (2019).
1017 55. Larson, R. C. *et al.* CAR T cell killing requires the IFNγR pathway in solid but not liquid
1018 tumours. *Nature* **604**, 563–570 (2022).
1019 56. Bailey, S. R. *et al.* Blockade or Deletion of IFNγ Reduces Macrophage Activation without
1020 Compromising CAR T-cell Function in Hematologic Malignancies. *Blood Cancer Discovery* **3**,
1021 136–153 (2022).
1022 57. Thibaut, R. *et al.* Bystander IFN-γ activity promotes widespread and sustained cytokine
1023 signaling altering the tumor microenvironment. *Nat Cancer* **1**, 302–314 (2020).

1024 58. Sotillo, E. *et al.* Convergence of Acquired Mutations and Alternative Splicing of CD19
1025 Enables Resistance to CART-19 Immunotherapy. *Cancer Discovery* **5**, 1282–1295 (2015).
1026 59. Domizi, P. *et al.* Ikaros Mediates Antigen Escape Following CD19 CAR T Cell Therapy in r/r B-
1027 ALL. *Blood* **138**, 613 (2021).
1028 60. Witkowski, M. T. *et al.* NUDT21 limits CD19 levels through alternative mRNA
1029 polyadenylation in B cell acute lymphoblastic leukemia. *Nat Immunol* **23**, 1424–1432
1030 (2022).
1031 61. Plaks, V. *et al.* CD19 target evasion as a mechanism of relapse in large B-cell lymphoma
1032 treated with axicabtagene ciloleucel. *Blood* **138**, 1081–1085 (2021).
1033 62. Fellmann, C. *et al.* An optimized microRNA backbone for effective single-copy RNAi. *Cell Rep*
1034 **5**, 1704–1713 (2013).
1035 63. Bloemberg, D. *et al.* A High-Throughput Method for Characterizing Novel Chimeric Antigen
1036 Receptors in Jurkat Cells. *Molecular Therapy - Methods & Clinical Development* **16**, 238–254
1037 (2020).
1038 64. Davila, M. L., Kloss, C. C., Gunset, G. & Sadelain, M. CD19 CAR-targeted T cells induce long-
1039 term remission and B Cell Aplasia in an immunocompetent mouse model of B cell acute
1040 lymphoblastic leukemia. *PLoS One* **8**, e61338 (2013).
1041 65. Jain, M. D. *et al.* Tumor interferon signaling and suppressive myeloid cells are associated
1042 with CAR T-cell failure in large B-cell lymphoma. *Blood* **137**, 2621–2633 (2021).
1043
1044
1045